Spring 1-1-2018

Large Eddy Simulations of Industrial Burners

Siddharth Prashant Nigam
University of Colorado at Boulder, siddharth.nigam1994@gmail.com

Large Eddy Simulations of Industrial Burners

by

Siddharth Prashant Nigam

B.S., University of New Hampshire, 2016

A thesis submitted to the

Faculty of the Graduate School of the

University of Colorado in partial fulfillment

of the requirements for the degree of

Master of Science

Department of Mechanical Engineering

2018

This thesis entitled:
Large Eddy Simulations of Industrial Burners
written by Siddharth Prashant Nigam
has been approved for the Department of Mechanical Engineering

_____
Prof. Peter E. Hamlington

_____
Prof. Gregory B. Rieker

_____
Prof. Nicole Labbe

Date _____

The final copy of this thesis has been examined by the signatories, and we find that both the content and the form meet acceptable presentation standards of scholarly work in the above mentioned discipline.

Nigam, Siddharth Prashant (M.S., Mechanical Engineering)

Large Eddy Simulations of Industrial Burners

Thesis directed by Prof. Peter E. Hamlington

During the past four years, a gift from 3M has funded a project that is at the intersection of academia and industry at the University of Colorado, Boulder (CU). The overall objective of this joint computational and experimental effort is to explore optimization and improvement of burner/chilled-roll systems for polymer film flame treatments. Using the computational and experimental tools developed in this project, existing treatment processes will be improved and new avenues of technology innovation will be explored.

In this thesis, industry-relevant heat treatment processes with catalytic and ribbon burners are studied using large eddy simulations (LES). The simulations are modeled in an open-source CFD package, OpenFOAM [1]. Different approaches are used to model chemistry in the simulations, from a single-step global mechanism to a detailed 41-step mechanism [2] for methane-air mixture.

The combustion of methane and boundary conditions are modeled to match the experimental setup at CU. Experimental data from wavelength modulation spectroscopy are used to estimate computational parameters and test the hypothesis of additional combustion in the catalytic burner to check whether the catalyst is working as expected. For the ribbon burner, there is some uncertainty about the initial conditions such as the inlet jet velocity and inlet temperature. In order to estimate those parameters, an inverse modeling approach is used in a gradient-based optimization study. Additional combustion is found to occur above the catalytic burner and initial prarmeters are estimated for the ribbon burner. This work will provide a toolkit for researchers at 3M to produce high fidelity simulations for their heat treatment processes.

Acknowledgements

Helpful discussions with Profs. Gregory Rieker, Nicole Labbe, and Daven Henze, as well as researchers Mark Strobel and Aniruddha Upadhye, are gratefully acknowledged. This work utilized gift funding from 3M and the Submmit supercomputer at the University of Colorado, Boulder.

This work would not have been possible without the help of my adviser, Peter Hamlington, whose mentorship and guidance are greatly appreciated. I would also like to acknowledge students from the Turbulence and Energy Systems Laboratory (TESLa) who have given me great feedback and resources. In particular, Jason Christopher, Caelan Lapointe, and Nicholas Wimer have helped tremendously and contributed to the work presented in this thesis. From the Laser Diagnostics Laboratory, Torrey Hayden and Daniel Petrykowski have provided experimental data and insight.

Finally, I would like to acknowledge my family for their support and Mimansa Thakar for her love and patience.

Contents

Chapter

Tables

Table

Figures

Figure

Chapter 1

Introduction

1.1 Motivation

Reacting flows are important in many natural and engineering systems and impact several aspects of human life. Forest fires, industrial burners, automobile engines, and other such systems involve the interaction between chemistry and fluid dynamics. It is important to understand these processes for various reasons, from improving efficiency to reducing pollution.

In most industrial applications involving combustion, the reactant (i.e., fuel and oxidizer) and product gases are turbulent, which adds another layer of complexity to an already complicated chemical kinetics problem. Turbulence generally results in an increase in mixing and thus increases the rate of combustion [8]. The heat release from combustion, conversely, results in temperature and density gradients that can influence the turbulence. Turbulence also introduces a wide range of spatial and temporal scales, whereas the chemistry of combustion introduces several equations to account for chemical species involved in the reactions. Therefore, understanding the interaction between chemistry and turbulence is of great interest to the scientific community. In the past, turbulent reacting flows have been studied extensively experimentally and analytically [9–11]. However, the improvement in the quality and availability of computational resources such as supercomputers and graphical processing units (GPUs) have increased the use of computations in both academia and industry [12, 13].

1.2 Project Overview

A gift from 3M has funded a project at the University of Colorado, Boulder (CU) over the last four years to characterize and, ultimately, optimize the performance of both catalytic and ribbon burners used in heat and chemical treatments of polymer films. The CU team, advised by Dr. Peter Hamlington and Dr. Gregory Rieker, has designed and fabricated a burner/chilled-roll experimental platform, used advanced laser-based diagnostics for in situ measurements of temperature and H_2O concentration above the catalytic and ribbon burners, and performed computational simulations for a range of burner/chilled-roll operating conditions. The primary objectives of the project are to expand the laser diagnostic measurement suite to include OH concentration, to experimentally characterize temperature and concentration fields in the region between the burner and chilled-roll for a range of conditions, to accurately reproduce and supplement experimental measurements using computational simulations for a range of conditions, and to computationally optimize the design and operating conditions of the burner/chilled-roll system for desired polymer film properties.

The overall objectives of this research are to characterize, optimize, and improve burner/chilled-roll systems for polymer film flame treatments. Through joint experimental and computational efforts, existing processes for polymer film treatments will be improved and new avenues of polymer treatment will be explored. Specific near- and long-term objectives of this project are to

- Develop an experimental platform, high-speed in situ laser diagnostics, and high resolution computational model to characterize and optimize burner/chilled-roll configurations, including those involving catalytic burners.
- Use computational simulations to study temperature uniformity, radical concentrations, and heat transfer at the film surface, as well as to understand the sensitivity of different parameters on the temperature and species concentration profiles.

- Use computational methods backed by experimental validation to rapidly explore a wide range of design and operational parameters and to improve the design and operation of burner/chilled-roll systems for the purpose of achieving specific flame treatment goals (e.g. increased speed, improved burner uniformity, and flame stability).
- Use computational simulations to perform optimization of the burner/chilled-roll design and operating parameters.

1.3 Thesis Scope

Industry-relevant heat treatment processes for films are characterized experimentally using wavelength modulation spectroscopy and computationally using large eddy simulations (LES) and direct numerical simulations (DNS). The scope of this thesis is to advance the computational modeling of both types of burner systems, the catalytic burner and the ribbon burner. Besides the geometry, the fundamental difference between the burners is the reaction region. For this study, both of the burners are characterized in the open configuration (i.e., without the roll). In the catalytic burner shown in Figure 1.1, the combustion of the premixed fuel ideally happens within the catalyst housing. The hot products then treat the polymer film on the roll.

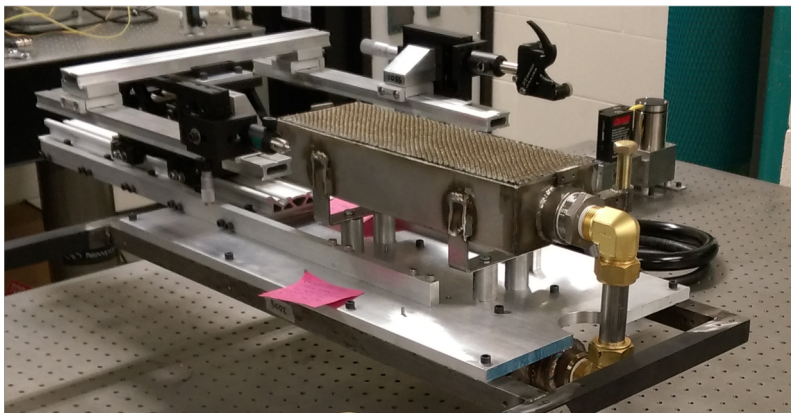

Figure 1.1: Experimental setup of the catalytic burner in the open configuration

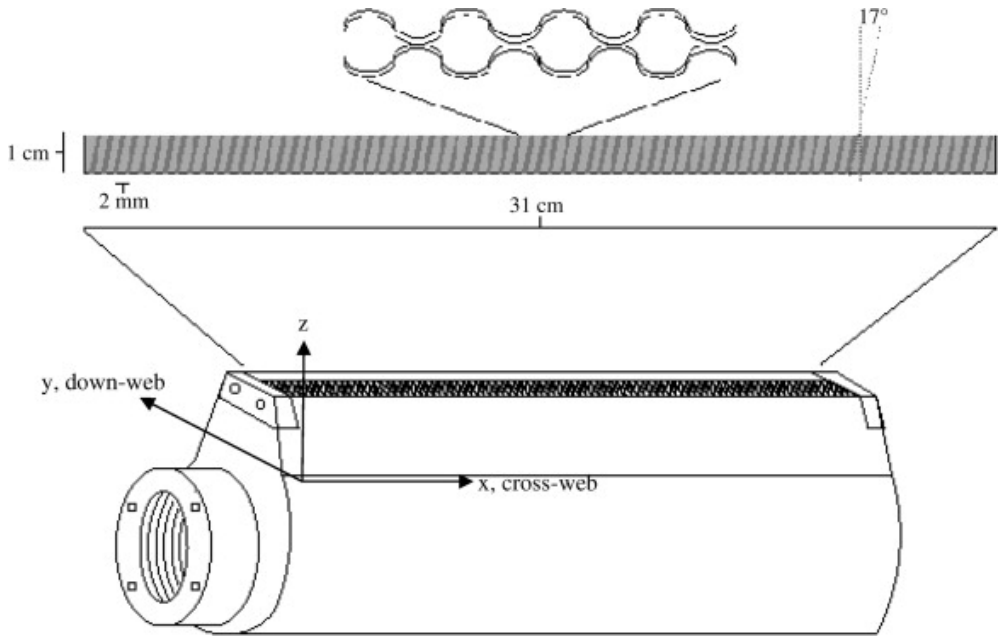

Figure 1.2: Schematic of the ribbon burner [3]

The combustion of the premixed fuel in the ribbon burner occurs above the housing. The use of corrugated stainless-steel sheets (called ribbons) creates several small ports, as shown in Figure 1.2. Premixed reactants of methane and air flow through these ports at a prescribed inlet temperature, velocity, and equivalence ratio. The combustion of this reactant mixture results in turbulent buoyant jets in the domain above the burner. The advantage to using such a ribbon pack, as opposed to a single port inlet, is that these ribbons provide higher flame stability and reduce the entrainment of cool ambient air [3]. Several factors impact the burner performance such as the flow velocity, the gap between the burner and the impingement surface (roll), and the port angle.

1.4 Organization

The rest of the thesis is organized as follows. The next chapter introduces the governing equations and the theoretical background for understanding reacting turbulent flows. Chapter 3 describes the tool used for the computational studies, OpenFOAM. In Chapter 4, the challenges with the catalytic burner are presented. In Chapter 5, a non-linear method of estimating experimental parameters for the ribbon burner is presented. Finally, conclusions and future work are outlined in Chapter 6.

Chapter 2

Theoretical Framework

In order to study turbulent reacting flows, we must first understand turbulence and chemical kinetics separately. This chapter presents some of the fundamentals of modeling premixed flames, both laminar and turbulent.

Laminar flows are smooth, ordered flows characterized by molecular diffusion as the primary mechanism of transport for temperature, momentum, scalars, and other properties across flow gradients. In contrast, turbulent flows are spatially and temporally complex and random. The complexity of turbulent flow enchances transport of the aforementioned properties and makes these flows well-suited for various engineering processes [8].

Whether a flow is laminar or turbulent is determined by the non-dimensional quantity called the Reynolds number, which is the ratio of the intertial to viscous forces in the flow [4], namely

$$Re = \frac{l_c v \rho}{\mu} \,, \tag{2.1}$$

where l_c is the characteristic length, v is the velocity of the flow, ρ is the density, and μ is the dynamic viscosity. Higher Reynolds number values correspond to turbulent flows, however the exact values for the transition from laminar to turbulent flow vary for different types of flow.

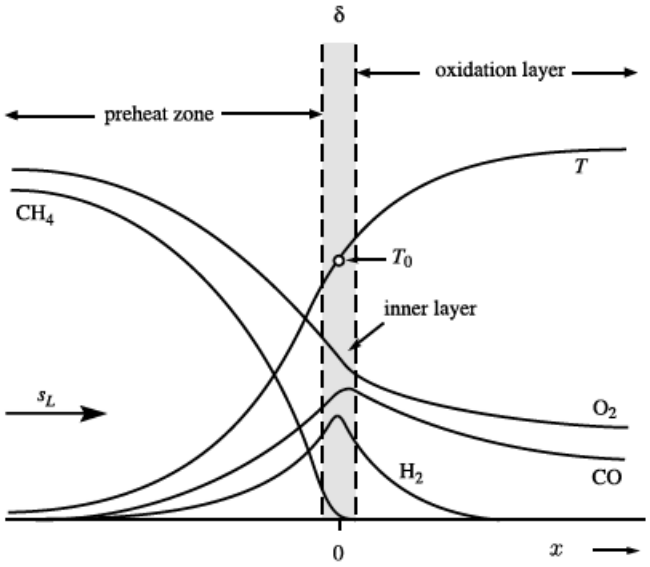

Figure 2.1: Temperature and major species for a laminar premixed methane-oxygen flame [4]

2.1 Laminar Premixed and Diffusion Flames

Laminar premixed flames have a relatively simple configuration. These flames are seen, for example, in many bunsen burners and can be characterized by a preheat zone, a reaction layer, and an oxidation zone, as shown in Figure 2.1.

In the chemically inert preheat zone, heat is transported mainly through conduction. The thin reaction layer is where the fuel consumption occurs. The thickness of the reaction region δ can be calculated from the temperature profile [5] as

$$\delta = \frac{T_2 - T_1}{\max(|\frac{\partial T}{\partial x}|)} \,, \tag{2.2}$$

In the oxidation layer, the final oxidation of the products occurs and the maximum temperature is achieved. This temperature is called the adiabatic flame temperature and for a stoichiometric mixture of methane and air, this temperature is 2240 K [5].

The speed at which a steady flow of premixed gas is normal to the flame front is the laminar flame speed, s_L. This is an important metric used for validating laminar premixed flame solvers and can be calculated analytically and experimentally [5].

The adiabatic flame temperature and other flame properties also depend on the ratio of fuel to oxidizer, known as the equivalence ratio [14]. The equivalence ratio is defined as

$$\phi = \frac{m_{fuel}/m_{ox}}{(m_{fuel}/m_{ox})_{st}} \tag{2.3}$$

where m_{fuel} is the mass of fuel (CH_4), m_{ox} is the mass of oxidizer (air), and the $(m_{fuel}/m_{ox})_{st}$ is the stoichiometric ratio of the mass of fuel and oxidizer. The mass ratio is stoichiometric when there is exactly enough oxidizer for all of the fuel to react. In the case of a methane-air mixture, an equivalence ratio of $\phi = 1$ corresponds to the exact amount of air needed to consume all of the methane. An equivalence ratio of $\phi < 1$ is fuel lean, where we have excess air, and an equivalence ratio of $\phi > 1$ is fuel rich, implying the presence of excess fuel. In most industrial applications, fuel lean streams are preferred since they are usually more cost efficient as fuels are generally more expensive than oxidizers.

Diffusion (or non-premixed) flames occur when the reactants (fuel and oxidizer) come in separate streams and depend on molecular mixing to come into contact and react. Thus, the flame speed for diffusion flames is limited by the rate of diffusion rather than the chemical rates [4]. Modeling fast chemistry is a good approximation for these flames since the chemical time scales are much faster than diffusion time scales. In this thesis, we will be dealing mostly with premixed flames.

2.2 Turbulent Flow

When the flow becomes turbulent, inertial forces dominate over stabilizing viscous forces. Thus, the flow becomes unstable and generates vortices at a higher rate than the viscous dissipation rate [15]. In order to characterize this flow, a turbulent Reynolds number is defined as

$$Re_T = \frac{v' l_T}{\nu} \,, \tag{2.4}$$

where v' is the velocity fluctuation (or turbulence intensity), ν is the kinematic viscosity, and l_T is the turbulent length scale. This turbulent Reynolds number is the ratio of turbulent transport to the molecular transport of momentum and characterizes how turbulent the flow is. When a turbulent flow interacts with a chemically exothermic reaction, there can be significant interplay between the two phenomena. The exothermicity of the reaction causes thermal expansion and stretching of the flame sheet. Turbulence also causes several smaller eddies to form that can cause wrinkling of the flame [16]. Figure 2.2 shows the wrinkling effect that a turbulent eddy with turblent length scale, l_T, has on the flame front propagating at laminar flame speed, s_L. This wrinkling can enhance the rate of the chemical reaction by increasing the flame surface area. In some cases, the turbulent flow can cut off the chemical reaction, resulting in flame quenching [4].

2.3 Governing Equations

In order to computationally model turbulent reacting flows, we need a closed system of equations. Most approaches to modeling such flows are finite-volume based approaches where the domain of interest is discretized into many smaller volumes. A closed system of equations is then solved for each small volume and for each time step. For the system of equations, we use the mass, momentum, and energy conservation equations along with equations of state. The governing equations for a Newtonian fluid are given below [4]. These equations represent the conservation of mass (Equation 2.5), conservation of momentum (Equation 2.6), conservation of

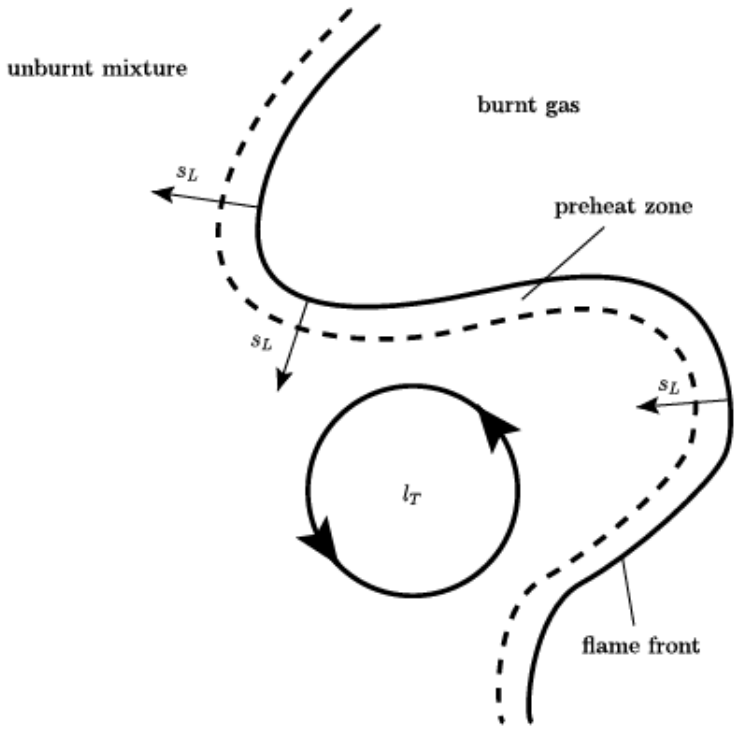

Figure 2.2: The effect of a turbulent eddy on the flame front [4]

energy (Equation 2.7), the conservation of species mass fraction (Equation 2.9), and the equation of state (Equation 2.10) namely

$$\frac{\partial \rho}{\partial t} + \frac{\partial}{\partial x_j}(\rho u_j) = 0 \,, \tag{2.5}$$

$$\frac{\partial}{\partial t}(\rho u_i) + \frac{\partial}{\partial x_j}\left(\rho u_i u_j + p\delta_{ij} - \tau_{ji}\right) = 0 \,, \tag{2.6}$$

$$\frac{\partial}{\partial t}(\rho e_0) + \frac{\partial}{\partial x_j}\left(\rho u_j e_0 + u_j p + q_j - u_i \tau_{ij}\right) = 0 \,, \tag{2.7}$$

$$\tau_{ij} = \frac{1}{2}\left(\frac{\partial u_i}{\partial x_j}\mu + \frac{\partial u_j}{\partial x_i}\right) - \frac{2}{3}\frac{\partial u_k}{\partial x_k}\mu\delta_{ij} \,, \tag{2.8}$$

$$\frac{\partial(\rho Y_\alpha)}{\partial t} + \frac{\partial(\rho u_j Y_\alpha)}{\partial x_j} = \frac{\partial}{\partial x_j}\left(\rho D \frac{\partial Y_\alpha}{\partial x_j}\right) + \dot{\omega}_\alpha \ , \tag{2.9}$$

$$p = \rho R T \ , \tag{2.10}$$

where ρ is the density, x and t are the spatial and temporal variables, u is the velocity vector, e_0 is the total energy density, p is the gas pressure, τ_{ij} is the viscous stress tensor, Y_α is the mass fraction of species α, $\dot{\omega}_\alpha$ is the chemical source term of species α, D is the mass diffusivity, R is the gas constant, and T is the temperature.

2.4 Turbulence Modeling

There are three main approaches to modeling turbulent flows:

(1) A direct numerical simulation (DNS) captures all relevant time and length scales of the turbulence. This is the most accurate way of modeling turbulent flow as it directly solves all of the conservation equations and there is no sub-grid scale modeling.

(2) A large eddy simulation (LES) captures the large scale turbulence features and models small scale features. For this approach, we use a filtered sub-grid scale model to capture the smallest turbulent features. These simulations are computationally cheaper than DNS and still capture most of the effects of turbulence on the flow.

(3) A Reynolds averaged Navier-Stokes (RANS) simulation is computationally the cheapest type of simulation but fails to capture nearly all of the spatial and temporal fluctuations. For these simulations, the fields of interest in the flow are decomposed into their mean and fluctuating parts and the conservation equations are averaged to solve for the mean parts of the flow. This approach gives a statistically significant ensemble average but fails to capture the instantaneous effects of turbulence on the flow.

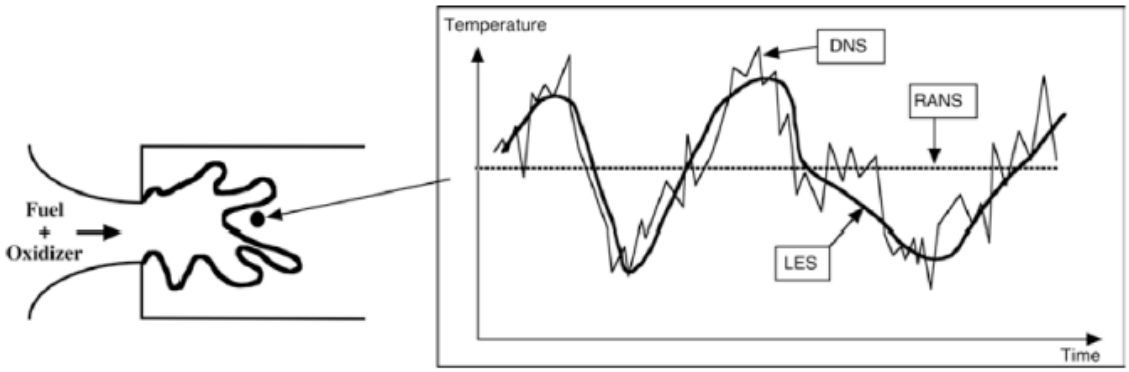

Figure 2.3: Time series of the temperature profile at a point with DNS, LES, and RANS methods [5]

For this study, we want to capture the instantaneous turbulence effects, model the chemistry, and use several simulations for a non-linear approach to parameter estimation. Figure 2.3 shows how the three approaches compare with each other. DNS is the most expensive since turbulent length scales can scale over orders of magnitude. In order to resolve the smallest features in the flow, the computational grid scales on the order of $(Re^{3/4})^3$ spatially and $Re^{1/2}$ temporally for three-dimensional flows [8]. When we introduce chemical kinetics to the flow, we have to track several species and introduce conservation equations for each species, thus adding significantly to the cost. While DNS is the most accurate approach, these simulations can take billions of CPU hours. Computationally, RANS simulations would be the most feasible from an optimization and cost approach, but we would fail to capture the instantaneous turbulence effects. For our studies for both the ribbon burner and the catalytic burner, we will use LES to capture the turbulence fluctuations as well as to optimize expermiental matching using several simulations and modeling the chemistry.

2.5 Modeling Chemistry

There are a few different ways of modeling the chemistry in reacting flow simulations. For our simulations, we use the following methods.

(1) Fast chemistry approach: In simulations where the chemical reaction time scale is a lot faster than the turbulence time scale, we can model the chemistry using an infinitely fast chemistry model. These models are not accurate at predicting all the species in detail since they only model a single-step global reaction. However, they can get accurate temperature and major species profiles if the Dahmköhler number is greater than 1. The Dahmköhler number relates the chemical reaction rate to the material transport rate [4].

(2) Arrhenius rate approach: Using this approach, we can limit the chemical reaction rate based on the Arrhenius rate equation [17].

$$k = Ae^{-E/RT} \,, \tag{2.11}$$

where k is the rate constant, A is the pre-exponential factor, E is the activation energy, R is the gas constant, and T is the temperature. This approach limits the chemical rate and thus the heat release and the chemical reaction are more evenly spread out in the domain. However, this is still a single-step reaction and cannot track intermediate species such as OH in methane-air combustion.

(3) Reduced order modeling: In simulations where the intermediate species profiles are desired, we can use reduced order models. These are usually models that are reduced from high fidelity chemistry mechanisms (such as the GRI 3.0 for methane-air combustion [18]) to predict profiles for different intermediate species. These models are generally multi-step and introduce several species to track using the solver. In Chapter 5, we look at a skeletal mechanism that consists of 16 species and 40 reactions [2].

(4) Detailed chemical mechanism: For finer details in the chemistry modeling, we can also look at using detailed chemical mechanisms. For the methane-air combustion reactions, the detailed mechanism is the GRI 3.0 mechanism that consists of 325 reactions and tracks 53 species [18]. Using this mechanism makes the simulation very expensive computationally and is generally avoided.

Chapter 3

Computational Setup

3.1 Computational Solver

The computational objective of this project is to develop high fidelity simulations that can aid in the design and optimization of two types of industrial burners, catalytic burners and ribbon burners. In this thesis, we use optimization methods to estimate inlet parameters for the ribbon burner. For the catalytic burner, the goal is to test the presence of additional combustion outside the burner.

The computations are performed in an open-source, C++ package called OpenFOAM [1]. It is a community driven database of various solvers ranging from turbulent combustion to molecular gas dynamics. For simulating reacting flows and turbulent buoyant jets, the most relevant OpenFOAM solvers are FireFOAM [19], reactingFOAM [1], and XiFOAM [1]. Of these solvers, only FireFOAM incorporates radiation modeling thus prompting its use for our simulations [7].

The intent of FireFOAM is to augment the current engineering prediction tools for fires. Before FireFOAM, most of the computational work in fire based simulations was done using Fire Dynamics Simulator (FDS) code [20] developed at the National Institute of Standards and Technology (NIST). Using radiation modeling, chemical species tracking, advanced chemistry mechanisms, higher order numerics, and pyrolysis modeling, FireFOAM has become a reliable solver for simulating fires and buoyant plumes. It is developed and used by the fire insurance company,

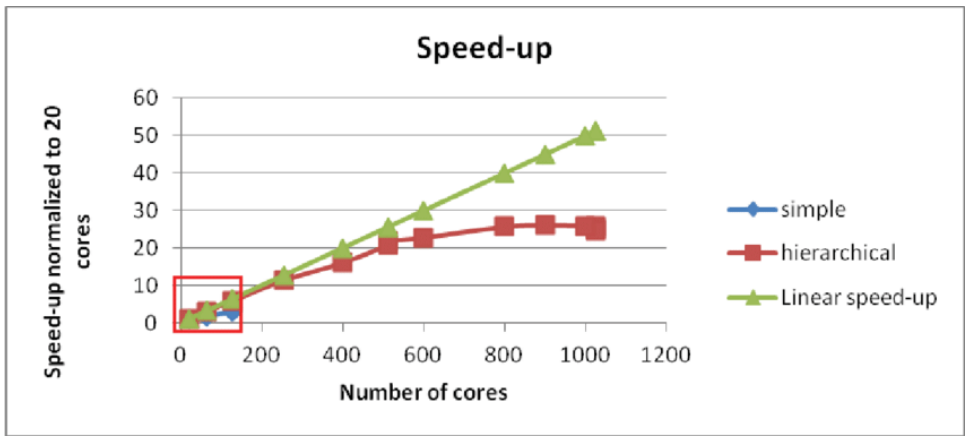

Figure 3.1: Model from Mazza et. al. [6] showing near-ideal scaling for simulations using OpenFOAM up to 1000 cores

FMGlobal, as their main tool for computationally predicting the characteristics of fires and for studying effective ways of mitigating and extinguishing such fires.

In terms of overall performance of OpenFOAM, it has been shown that OpenFOAM has nearly ideal scaling to large numbers of processors [21]. For the simulations presented in this study, we scaled the runs to up to 12 processors locally and up to 144 processors on the CU Supercomputer, Summit [22]. The red box in Figure 3.1 shows the linear scaling of OpenFOAM up to those conditions.

3.2 Computational Mechanics

OpenFOAM has many built-in physics modules, making it ideal for quickly simulating a broad range of problems. Since OpenFOAM is freely available, we anticipate that this choice of code will facilitate the transfer of simulation capabilities developed at CU to researchers at 3M. Eventually, we would like to provide a computational tool that can be run by 3M researchers locally on their desktop workstations.

The computations performed are large-eddy simulations (LES), which allows three dimen-

sional variations in the flow field to be resolved both temporally and spatially. LES directly resolves large-scale motions in the flow while modeling small scales, and thus strikes an ideal balance between computational efficiency and physical accuracy. The temporal and spatial accuracy of LES also makes it an ideal method for studying variations in temperature and chemical species fields above catalytic and ribbon burners. Averaged approaches such as those based on the Reynolds-averaged Navier Stokes (RANS) equations fail to completely represent the local and instantaneous variability in the flow, and are often performed in only two dimensions, whereas the real-world flow field is highly three dimensional.

FireFOAM is a fully compressible solver and, as mentioned in the previous chapter, it uses the Favre filtered Navier-Stokes equations [23] to solve for the fluid flow. Using the conservation equations (Equations 2.5, 2.6, and 2.7) described in Chapter 2, we can derive the Favre filtered equations given below.

$$\frac{\partial \overline{\rho}}{\partial t} + \frac{\partial}{\partial x_j}(\overline{\rho}\widetilde{u_j}) = 0 \,, \tag{3.1}$$

$$\frac{\partial}{\partial t}(\overline{\rho}\widetilde{u_i}) + \frac{\partial}{\partial x_j}\left(\overline{\rho}\widetilde{u_i}\widetilde{u_j} + \overline{p}\delta_{ij} - \widetilde{\tau_{ji}^{tot}}\right) = 0 \,, \tag{3.2}$$

$$\frac{\partial}{\partial t}(\overline{\rho}\widetilde{e_0}) + \frac{\partial}{\partial x_j}\left(\overline{\rho}\widetilde{u_j}\widetilde{e_0} + \widetilde{u_j}\overline{p} + \widetilde{q_j^{tot}} - \widetilde{u_i}\widetilde{\tau_{ij}^{tot}}\right) = 0 \,, \tag{3.3}$$

$$\widetilde{\tau_{ij}^{tot}} = \widetilde{\tau_{ij}^{lam}} + \widetilde{\tau_{ij}^{turb}} \,, \tag{3.4}$$

$$\widetilde{\tau_{ij}^{lam}} = \mu\left(\frac{\partial \widetilde{u_i}}{\partial x_j} + \frac{\partial \widetilde{u_j}}{\partial x_i} - \frac{2}{3}\frac{\partial \widetilde{u_k}}{\partial x_k}\mu\delta_{ij}\right) \,, \tag{3.5}$$

$$\widetilde{\tau_{ij}^{turb}} = -\overline{\rho u_i'' u_j''} \,, \tag{3.6}$$

where ρ is the density, x and t are spatial and temporal variables, u is the velocity vector, e_0 is the total energy density, p is the gas pressure, and $\widetilde{\tau_{ij}^{turb}}$ is the turbulent component of the stress tensor that is modeled to close the system of equations along with the equation of state (Equation 2.10).

As with other reacting flow solvers, the total energy equation is in terms of total enthalpy. Species mixing is tracked using transport equations for the mixture fraction, which is treated as a conserved scalar (Lewis number of unity). Since it is a LES solver, closure is needed for the sub-grid scale stress. In the case of FireFOAM, it is modeled by the eddy viscosity concept using a one-equation model [7]. It should be noted that other models can be used for this closure as well, such as the Smagorinsky model. Radiation is also modeled in these simulations, and FireFOAM can use several different radiation models such as P1 (assumes a large optical thickness for flames) or fvDOM (finite volume discrete ordinate method). For the current study, we assumed an optically thin flame with a constant radiant fraction of 20%, as estimated by McCaffrey [24].

Since these are LES, they are already more tractable than DNS and can be made computationally cheaper using techniques such as static mesh refinement (SMR) for the computational domain and reduced order modeling (ROM) for the chemical kinetics. The relatively modest size of these simulations permits a large parameter space to be explored; such a parameter space is necessary in order to develop the parameterizations that are the ultimate objective of this project.

In terms of the numerical methods applied, OpenFOAM uses the finite volume method on unstructured or structured mesh using pressure based solvers. This method is similar to the commercial CFD codes such as Ansys Fluent and Star CCM. Since OpenFOAM is open source and highly customizable, there are several numerical schemes that can be used for any simulation. The time stepping is adaptive and based on the Courant number. A rule of thumb is to have a Courant number below 0.5 in simulations for good convergence. The Courant number is a dimensionless

quantity defined as

$$C = \frac{u_x \, \Delta t}{\Delta x} + \frac{u_y \, \Delta t}{\Delta y} + \frac{u_z \, \Delta t}{\Delta z} \, , \tag{3.7}$$

where u is the velocity of the flow in the smallest cell in a given direction, Δt is the time step of the solver, and Δx, Δy, and Δz are the lengths of the smallest cells in the respective directions. This value affects the convergence of a simulation. Physically, a maximum Courant number greater than one within one timestep implies that in certain parts of the simulation, the fluid flow spans more than a cell in the domain, implying that the said cell will be skipped in that iteration of the solver. This is why it should always be below 1. For these simulations, the Courant number is set to 0.4 and PISO and SIMPLE algorithms are used to couple separate equations [25].

3.3 Static Mesh Refinement

One method of reducing the computational cost of simulations is by using the technique of static mesh refinement (SMR). Using a priori information about the flow structure, we can make certain regions more computationally refined than others instead of having a uniform grid in the entire domain. In our simulations, the region near the inlet requires a highly resolved grid to properly capture the physics in the small scales. Further away, in the far field region, the grid resolution does not have to be as refined as that in the near field. Thus, we can use that information to improve results in the near field without increasing the cost of the simulation too much. We used grading in order to achieve that. In OpenFOAM, we can prescribe a certain value of grading which determines the expansion ratio. A grading of $(1\ 10\ 1)$ will result in a domain where the last cell in the y direction is 10 times taller than the first cell in the y direction. The cells in x and z directions remain unaffected and stay uniform throughout the domain. Grading can also be used to create fine scales in the domain in multiple directions. In our case of modeling turbulent combustion for the different inlets, flames are often in the middle of the domain. In

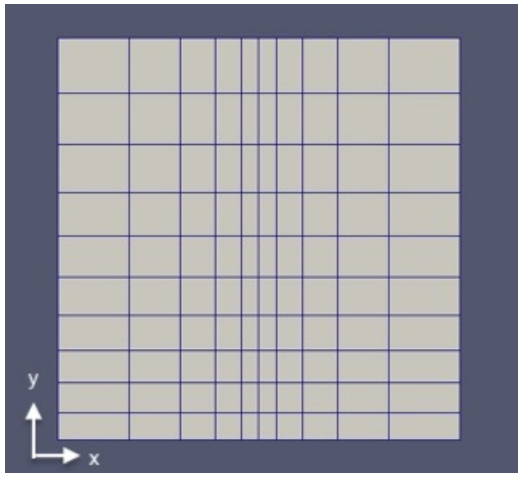

Figure 3.2: Static mesh refinement using a grading of (4 2) in a square domain

such cases, it is desirable to have the finest resolution in the center of the domain near the inlet of the premixed gases. BlockMeshDict in OpenFOAM allows users to create such domains with custom resolution as shown in Figure 3.2. That figure shows a square domain with a grading of (4 2) with the 4 in the x direction being applied at the center of the domain. We also used another software, Pointwise, to generate mesh and implemented static mesh refinement.

3.4 Validation of FireFOAM

The creators of FireFOAM [7] simulated five methane fires resulting from a 0.3 m $\times$ 0.3 m square inlet in a domain of 3 m $\times$ 3 m $\times$ 3 m with varying heat release rates as shown in Table 3.1. $Q*$ and $D*$ are non-dimensional heat release rates and the characteristic length scale and are used for scaling and grid resolution studies in other CFD simulations [26, 27]. Using the OpenFOAM meshing utility called SnappyHexMesh, the domain is split up into four refinement levels. The finest refinement is in the middle right above the burner surface. This region has uniform cells of 1.25 cm $\times$ 1.25 cm $\times$ 1.25 cm and is bounded in a 0.6 m $\times$ 1 m $\times$ 0.6 m box. This region (level one) bounds the continuous flame region and it is the most important region to predict accurately because of the sub-grid scale effects thus having the smallest sized cells. Level

two refinement has a cell size of 2.5 cm $\times$ 2.5 cm $\times$ 2.5 cm and is the plume region bounded by a 1.2 m $\times$ 2 m $\times$ 1.2 m box and the level one refinement box. Proportional scaling for the other two levels results in a cell size of 10 cm $\times$ 10 cm $\times$ 10 cm at the outermost boundaries of the domain. The simulations are performed for 20 s and the last 13 s are used for the turbulence statistics.

Table 3.1: Simulation cases where $Q*$ and $D*$ are non-dimensional heat release rates and the characteristic length scale

	HRR (kW)	Q*	D*
Case 1	14.4	0.1926	0.1752
Case 2	21.7	0.2903	0.2064
Case 3	33.0	0.4414	0.2441
Case 4	44.9	0.6006	0.2761
Case 5	57.5	0.7691	0.3049

The first validation test was to check the conservation of energy in the simulation domain. In order to test that, the total enthalpy flux was integrated for planes at different heights in the domain (every 10 cm) and averaged over time. One important observation was the decrease in the chemical enthalpy flow rate with an increase in height, which was active in the flame zone (level one). In the regions above the flame zone, the enthalpies (both total and chemical) remain constant, showing numerical conservation of enthalpy and species.

FireFOAM performs reasonably accurately when comparing the centerline temperature and velocity data from the simulations to the experimental results and scaling laws. Figure 3.3 shows the change in the centerline mean temperature and compares it to McCaffrey's results and scaling laws [24]. The figure below shows the three distinct regions that are also observed experimentally. The first region with the constant temperature rise is the continuous flame zone (from $Y/\dot{Q} =$ 0 to 0.08) followed by a -1 decay in the intermittent zone (from $Y/\dot{Q} = 0.08$ to 0.2), and with a $-1/3$ decay in the plume zone (from $Y/\dot{Q} > 0.2$). The simulation over-predicts the calculated peak temperature by $250 - 350$ K but that is attributed to the lack of correction of the experimen-

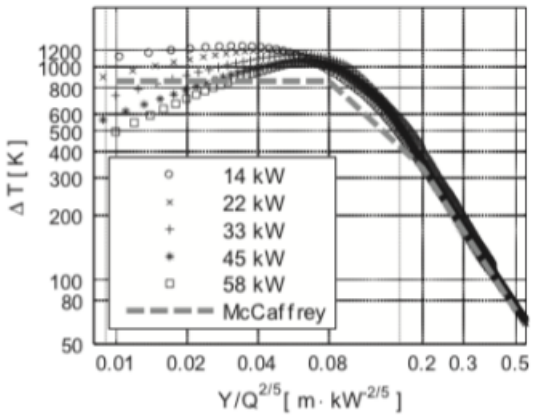

Figure 3.3: Centerline mean temperature rise for the validation cases for FireFOAM [7]

tal data for thermocouple radiation. According to McCaffrey, the flame temperatures estimated were under-predicted on the order of 20% because of the thermocouple radiation [24].

Looking at the centerline fluctuations provided good insights into the advantage of using LES models over RANS models. Using only the 58 kW case, the authors showed that the sub-grid scale fluctuation of the mixture fraction is about 15-30% of the resolved fluctuation in the continuous flame region and slightly lower at 10-15% in the intermittent region [7]. This proves that the LES model used captures the majority of the mixture fraction fluctuations making that much less sensitive to the turbulence model selected than the RANS simulations.

Chapter 4

Catalytic Burner

4.1 Catalytic burner setup

The catalytic burner is a type of system where the catalyst aids the chemical reactions. These burners are designed to have the fuel combustion reactions within the catalyst housing and the products that exit are already at a high temperature to treat the polymer film. Ideally, there are no radicals exiting the catalyst since the combustion reactions occur within the catalyst housing. In our simulations, the catalytic burner is modeled as a rectangular inlet. For the two-dimensional simulations, the inlet is modeled as a line source where the products from the combustion come from the inlet as shown on the left schematic in Figure 4.1.

4.2 Initial and Boundary Conditions

As mentioned in Chapter 2, in order to close the system of equations for our solver, we need to define initial and boundary conditions. One of the main challenges for computations is to accurately represent the initial and boundary conditions. In some cases, the initial conditions can be easily measured or estimated. However, for complex geometries such as the ribbon burner, they are harder to estimate. Chapter 5 presents those details.

Figure 4.1 shows the catalytic burner domain in order to understand the boundary conditions. To model the experimental setup, we need to allow for the entrainment of air from all

sides of the domain. This is achieved through a special boundary condition in OpenFOAM that models the hydrostatic pressure field as the reference state for the edges of the domain where this boundary condition is applied. This provides an accurate measurement of entrainment in large domains [28]. The other boundary conditions are shown in Table 4.1. The OpenFOAM boundary condition $inletOutlet$ is a combination of the conditions $zeroGradient$ and $fixedValue$ in which case the flow features (such as velocity) at that boundary pointing into the domain are modeled as a fixed value prescribed at the inlet thus replicating the $fixedValue$ boundary condition and the flow features pointing out of the domain are approximated as the same values at the cells closest to the edge similar to the $zeroGradient$ condition. The boundary conditions for the field, front and back, are empty in two-dimensional simulations since OpenFOAM does not natively solve in two-dimensions. The entire domain for 2D simulations is what is shown on the left schematic in Figure 4.1. In three-dimensional simulations, the front and back faces have the same boundary conditions as the sides, i.e., the open boundary conditions that allow for entrainment.

Table 4.1: Boundary conditions for 2D catalytic burner simulations

Geometry	Top	Sides	Base	Inlet	Front and Back
T (K)	inletOutlet			fixedValue (300)	empty
P_{rgh} (Pa)	prghTotalHydrostaticPressure			fixedFluxPressure	empty
U (m/s)	inletOutlet inlet = (0 0 0)	pressureInletOutletVelocity		fixedValue (0 0.5 0)	empty

4.3 Methane Sensitivity

The fuel used in the catalytic burner is methane and the oxidizer is air. Using the experimental equivalence ratio of $\phi = 0.85$, we calculated the mass fractions of different species for the given reaction using NASA Chemical Equilibrium with Applications (CEA) [29] and initialized

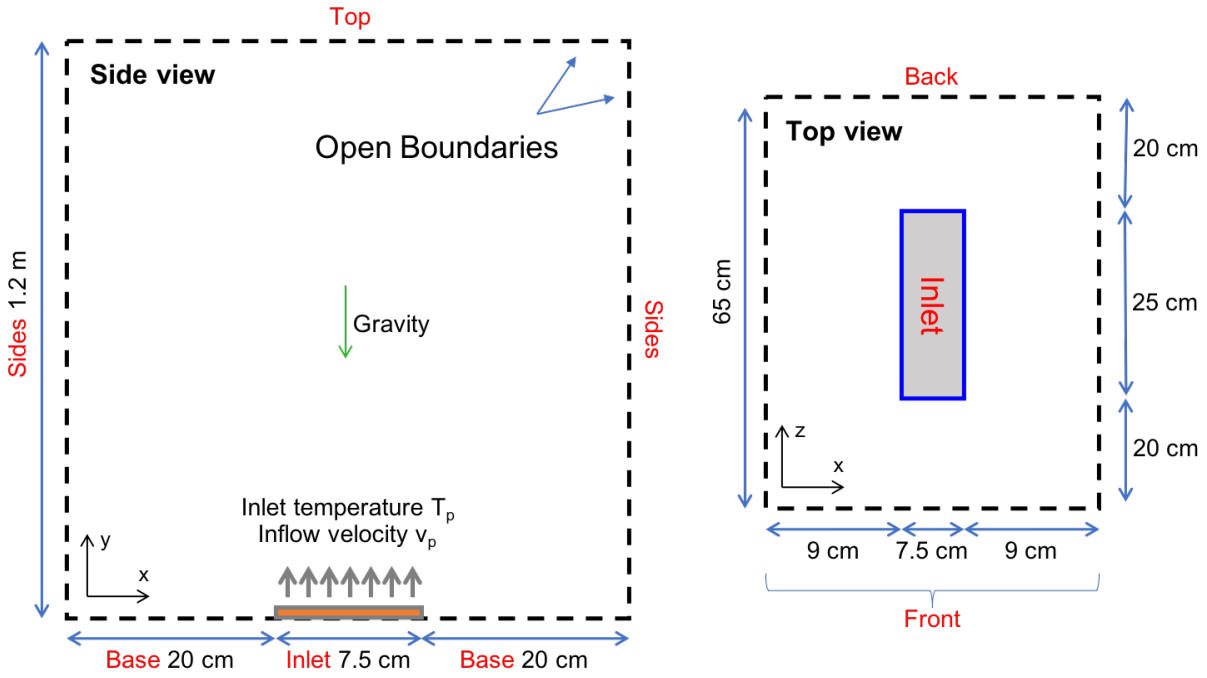

Figure 4.1: Computational domain for the catalytic burner with boundaries from Table 4.1 shown in red

our simulations with those values for the mass fractions of the major chemical species. Experimental results showed higher values in the temperature profile above the burner when compared to the simulations. A possible reason for this discrepancy could be the assumption that there was complete combustion of methane in the burner. In order to test that hypothesis, we can conduct a sensitivity analysis and see how the temperature profile changes with the addition of small amounts of methane.

4.3.1 Parameter Calculation

In order to study the sensitivity to trace amounts of unreacted methane in the domain, we ran simulations where the species mass fractions were initialized by NASA-CEA and a trace amount of methane was added into the domain through the inlet. The overall reaction is given

by Equation 4.1.

$$CH_4 \ + \ 2\,O_2 \ + \ 7.52\,N_2 \ \rightarrow \ CO_2 \ + \ 2\,H_2O \ + \ 7.52\,N_2 \tag{4.1}$$

In CEA, we assumed that there is complete combustion, which is why CH_4 is not in the products side. We also ignored other species that CEA output (Ar, CO, H, H_2, NO, N_2, O, and OH). These species were ignored because either their mole fractions were too low (e.g. H, H_2, O) or it was determined that they do not play an important role in the temperature profile post the reaction (e.g. Ar, N_2). Nitrogen gas was used to balance any missing terms from the mass fraction so that the sum of all the mass fractions was 1. The species from the reaction that were taken into consideration were O_2, CO_2, H_2O, and N_2. Figure 4.2 shows the mass fractions of all the products from Equation 4.1.

4.3.2 Sensitivity Runs

The simulations were run for 30 s with a time-step of 10^{-5} s The inlet temperature was set at 1580 K to match the experimental setup, and an equivalence ratio of $\Phi = 0.85$ was used. The simulation was two-dimensional with a domain of 0.5 m $\times$ 1.2 m, a resolution of 65 $\times$ 90 with grading of (1 10), and a Courant number of 0.5. The boundary conditions for the simulation are given in Table 4.1. Five simulations were run with varying amounts of methane (mass fraction of 0, 0.001, 0.003, 0.005, and 0.010). For reference, a mass fraction of 0.047 is the amount of methane in a reaction with an equivalence ratio of $\Phi = 0.85$. We used both single-step chemistry (with the fast chemistry approximation) as well as a higher fidelity skeletal mechanism to model the chemistry in the simulations. For the baseline case of a 2D domain with a single-step reaction, the temperature and water mole fraction profiles are shown in Figure 4.3. We can see that there is a strong correlation between the temperature and the water mole fraction profiles. This is encouraging because the experimental results also show that the water mole fraction and temperature profiles have the same trends.

```
prob case=29835988  hp p(atm)=1
phi=0.85
reac
 fuel  CH4             wt%= 100.0 t,k= 300.00
 oxid Air              wt%= 100.0 t,k=298.15
output short
output trace= 1e-5
end

        THERMODYNAMIC EQUILIBRIUM COMBUSTION PROPERTIES AT ASSIGNED

                                PRESSURES

CASE = 29835988

            REACTANT                    WT FRACTION      ENERGY      TEMP
                                         (SEE NOTE)     KJ/KG-MOL      K
FUEL         CH4                         1.0000000    -74533.907    300.000
OXIDANT      Air                         1.0000000      -125.530    298.150

O/F=   20.28061  %FUEL=  4.699112  R,EQ.RATIO= 0.850228  PHI,EQ.RATIO= 0.850000

THERMODYNAMIC PROPERTIES

P, BAR             1.0132
T, K             2067.59
RHO, KG/CU M    1.6425-1
H, KJ/KG         -222.45
U, KJ/KG         -839.36
G, KJ/KG        -20081.5
S, KJ/(KG)(K)     9.6049

M, (1/n)          27.866
(dLV/dLP)t      -1.00061
(dLV/dLT)p        1.0200
Cp, KJ/(KG)(K)    1.6780
GAMMAs            1.2260
SON VEL,M/SEC      869.7

MOLE FRACTIONS

*Ar             8.5864-3
*CO             1.1064-3
*CO2            8.0811-2
*H              5.4141-5
*H2             4.5850-4
H2O             1.6156-1
*NO             3.1495-3
*N2             7.1434-1
*O              1.8145-4
*OH             2.4178-3
*O2             2.7332-2

 * THERMODYNAMIC PROPERTIES FITTED TO 20000.K

NOTE. WEIGHT FRACTION OF FUEL IN TOTAL FUELS AND OF OXIDANT IN TOTAL OXIDANTS
```

Figure 4.2: Chemical equilibrium output to initialize the catalytic burner simulations

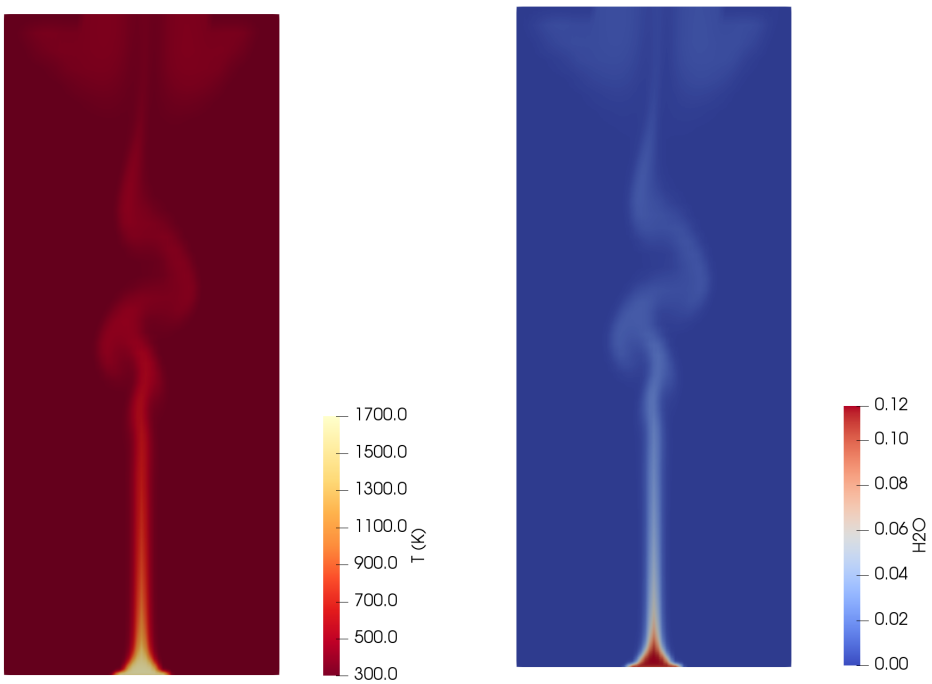

Figure 4.3: Temperature (left) and water mole fraction (right) profiles for a 2D catalytic burner case

4.3.3 Analysis

We were interested in the temperature profile and the water mole fraction above the burner. We can see from Figures 4.4 and 4.5 that even a small amount of methane can increase the temperature and the mole fraction of water. This supports the hypothesis that there might be some unburned methane that goes through the burner and enters the domain. This methane then continues to undergo combustion above the burner, thus causing an increase in the temperature. The combustion of methane also produces water vapor, which can be seen in Figure 4.5. This gives us further insight into the trends we observe experimentally that the temperature does not immediately start to drop off above the burner. Both the plots are for single-step chemistry. We can see that there is a significant difference in the near field temperatures for the different cases. This is because of the fast chemistry approximation. Since the reactants are already premixed (methane-air mixture coming from the inlet), combustion occurs as soon as the reactants enter the domain. That causes the temperature near the base to increase proportionally to the amount of methane entering the system as shown in Figure 4.4.

When we increase the fidelity of chemistry in our simulations, the profiles collapse and converge more in the near field and the reactions occur as we get higher into the domain, followed by another convergence to similar far field values for both the fields. Figure 4.6 shows the temperature and water mole fraction profiles in the multi-step chemistry (41 steps, 16 species) simulation. When compared with the single-step chemistry plots shown on the right, it can be seen that the magnitude of difference in the temperature profiles at different concentrations of unreacted methane has decreased. However, the increase in these profiles still suggests that there could be additional unreacted methane that flows out of the catalytic burner and reacts in the domain above. These additional reactions are problematic because the radicals that are produced as part of the oxidation of methane, such as OH, can react with the polymer film and produce undesirable inconsistencies in the treated film.

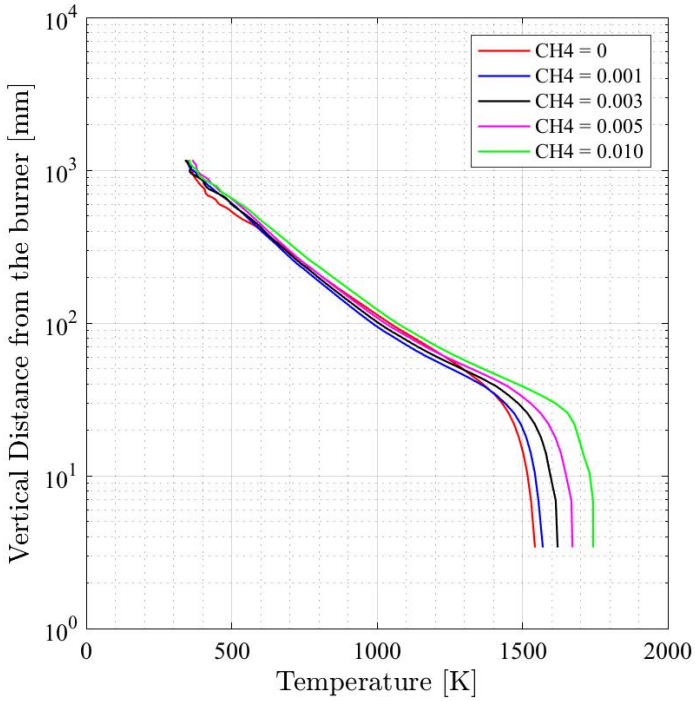

Figure 4.4: Temperature as a function of height for different amounts of unreacted methane entering the domain using single-step chemistry

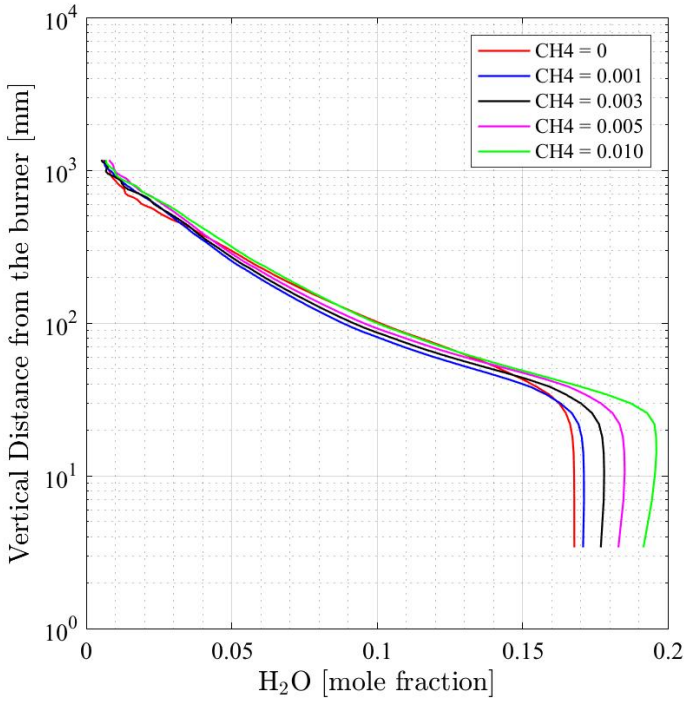

Figure 4.5: Water mole fraction as a function of height for different amounts of unreacted methane entering the domain using single-step chemistry

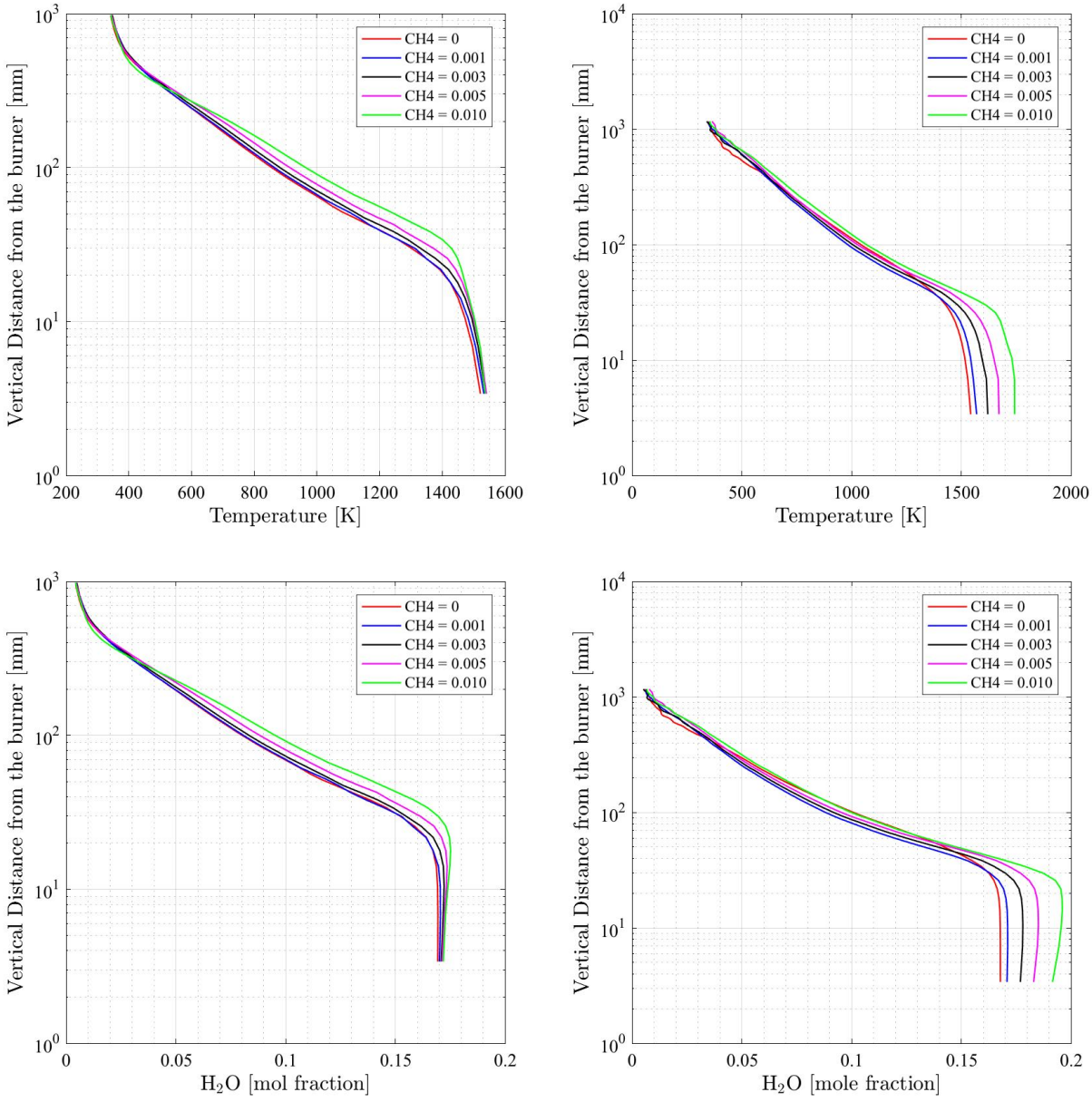

Figure 4.6: Temperature (top) and H_2O mole fraction (bottom) profiles for advanced (left) and single-step chemistry (right) models

Using advanced chemistry models, we can track other species of interest such as OH which was not possible with the single-step chemistry model. Figure 4.7 shows the OH mole fraction as a function of the vertical distance from the center of the burner. From the Figure, it is evident that the magnitude of OH for different CH_4 concentrations is highly sensitive. The OH mole fraction almost doubles in magnitude between the first and the last concentrations of CH_4. Since OH is a highly reactive species, we are interested in knowing the trends it follows because it can impact the heat treatment process by reacting with the polymer film.

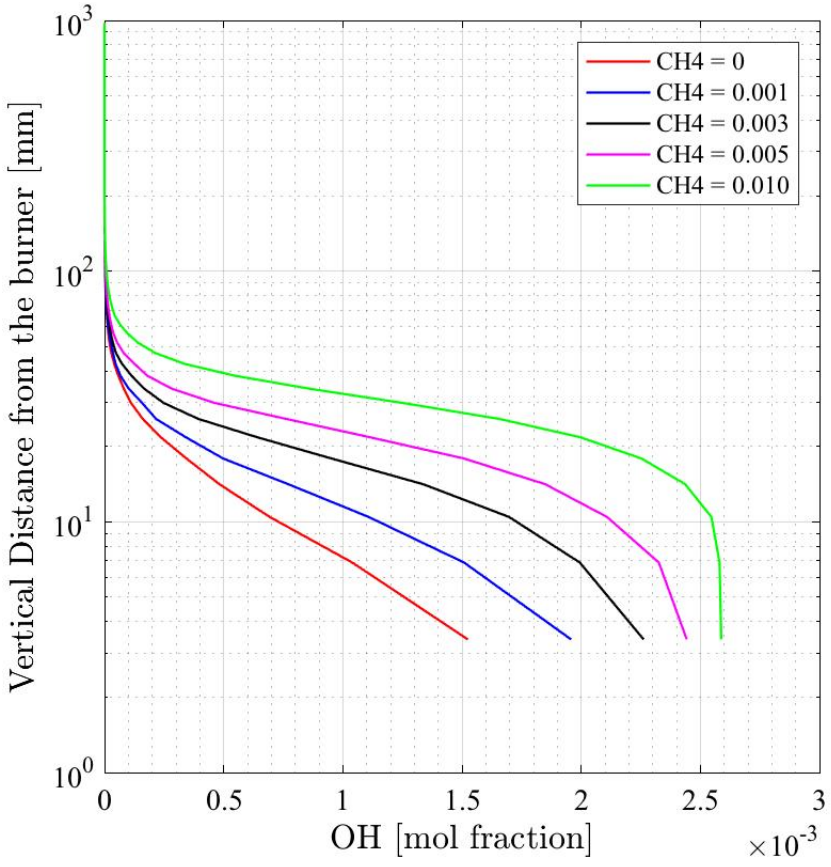

Figure 4.7: OH mole fraction as a function of height in different cases

Chapter 5

Ribbon Burner

5.1 Ribbon burner setup

This study is the first step towards developing high fidelity simulations for the ribbon burner. The main objective of this study is to accurately predict the temperature profile for the combustion of a methane and air mixture over a ribbon burner.

The experimental setup for the ribbon burner is shown in Figure 5.1. A chilled cylindrical roll is placed above the ribbon burner and film is passed on the roll. Using wavelength modulation spectroscopy, we can measure the temperature and certain species profiles. The initial simulations to validate the computational fluid dynamics (CFD) models are designed to study the domain above the burner without the roll, referred to as the open ribbon burner configuration.

5.2 Initial and Boundary Conditions

As mentioned in Chapter 2, the complex geometry of ribbon burners poses a challenge to the modeling of its initial and boundary conditions.

The computational domain is shown in Figure 5.2. We only model a small but repeated section of the ribbon burner. Since the burner is thin and long, we estimate that we can simulate a small section and use periodic boundary conditions to model the burner. For this study, we are

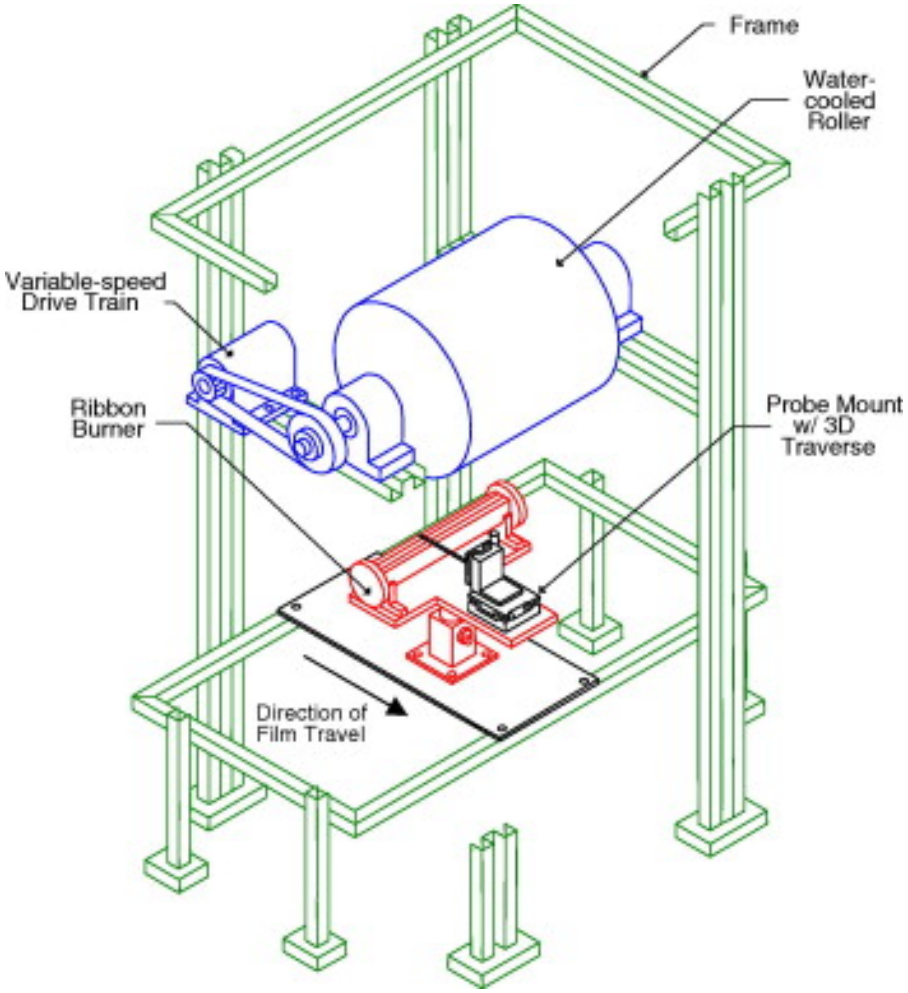

Figure 5.1: Schematic of ribbon burner experimental setup [3]

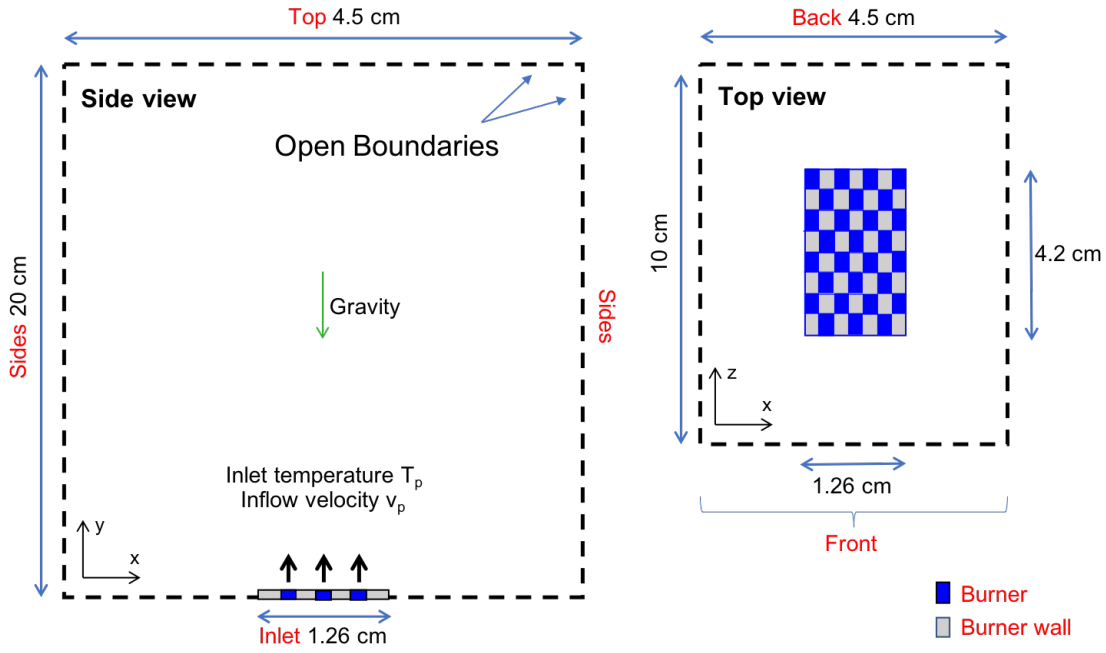

Figure 5.2: 3D computational domain of the ribbon burner with the boundaries marked in red

only modeling a small section of the burner and allowing the domain to be large to account for entrainment of air. The centerline statistics should be comparable to the experimental centerline profiles using this approach. Besides the inlet, the boundary conditions are the same for both types of burners. For the ribbon burner inlet, the burners are modeled as inlets through which the premixed reactants come in at a prescribed temperature, velocity, and equivalence ratio. The burner walls are modeled as walls that are at a high initial temperature to model the stainless-steel ribbon walls.

5.3 Modifying the Simulations

Using a non-linear gradient-based optimization approach has certain disadvantages. Since the parameters for each simulation are based on the gradient determined from previous simulations, we can only parallelize each individual simulation and not run an ensemble of simulations

Table 5.1: Boundary conditions for 3D ribbon burner simulations

Geometry	Top	Base and Sides	Burner	Burner Wall
T (K)	inletOutlet		fixedValue (300 K)	fixedValue (600 K)
P_{rgh} (Pa)	prghTotalHydrostaticPressure		fixedFluxPressure	fixedFluxPressure
U (m/s)	inletOutlet inlet = (0 0 0)	pressureInletOutlet	fixedValue (0 1.0 0)	noSlip

on several cores of a supercomputer. This means that in order to get a large number of simulations done for parameter estimation in a timely manner, we must reduce the cost of our simulations. This is done in three ways:

(1) By reducing the resolution of the mesh: Using techniques like static mesh refinement and grid stretching, we are able to cut down the cell count of these simulations from 200,000 cells to about 80,000 cells.

(2) By reducing the number of equations to solve at each time step: We do this by modeling the chemistry with a single-step global mechanism.

(3) By reducing the end time for each simulation: We need to get converged statistics but we cannot run each simulation for 30 s locally since solving for each second takes about 50 CPU hours. Using a 12 processor machine, we can solve for a second of data in about 4 hours. In order to test the convergence time of these simulations, we plot the centerline mean temperature profiles at different times and see when they collapse implying that the earliest time in the collapsed region would be the shortest amount of time we can run our simulations for. To do this, we ran the simulation that would take the longest to converge, i.e., the simulation with the highest inlet velocity and the lowest inlet temperature. Figure 5.3 shows that 1 s of run time for these simulations should be good for converged statistics.

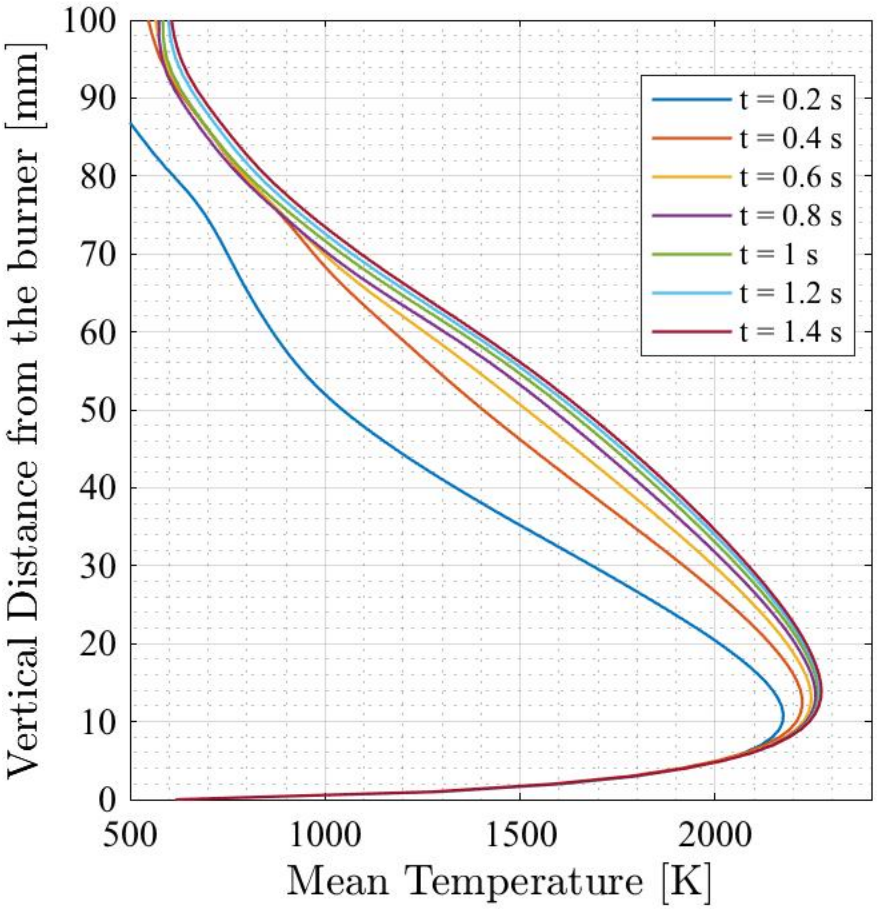

Figure 5.3: Testing the convergence of temperature for different run times for the ribbon burner

5.4 Test Simulation

Before we analyze results from the parameter estimation study, we need to look at a test simulation of the ribbon burner. Figure 5.4 shows a snapshot from a simulation that is the starting point of the parameter estimation study. We can see the pulsating behavior in both the 3D and the 2D temperature profiles. The flame is leaning to the right because of the 17° angle of the ribbon burner ports. These ports are angled to prevent the slipping of ribbon packs since they are only pressed together and spot welded to keep them in place. The temperatures seem to be in the physical range as well, given that the adiabatic flame temperature of methane is 2240 K [5].

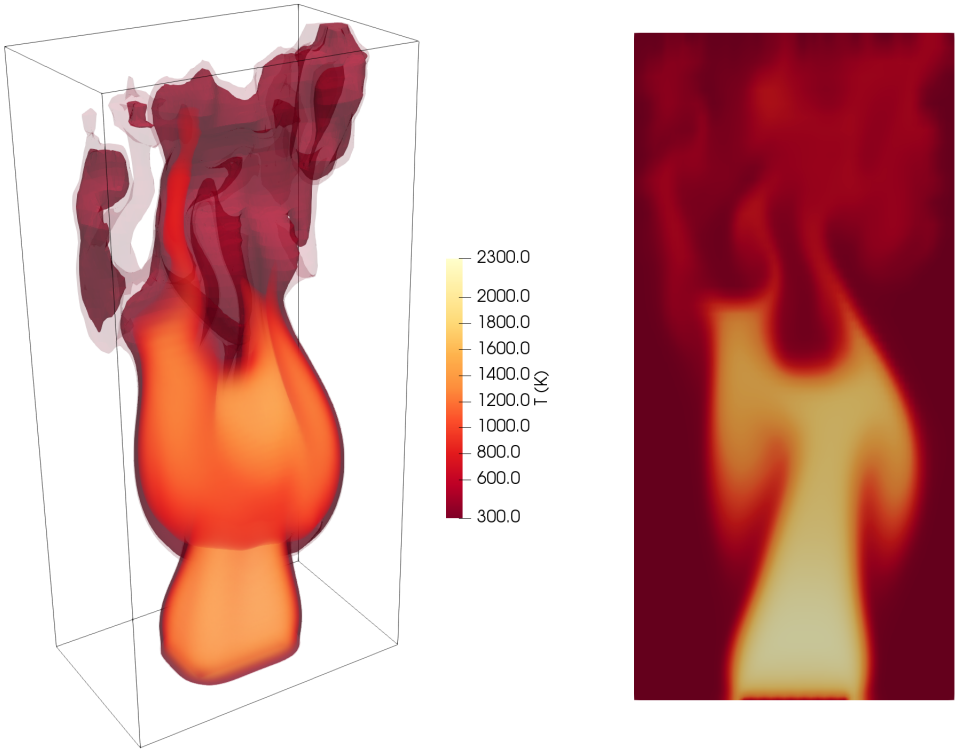

Figure 5.4: Snapshot of a 3D ribbon burner simulation with the 3D temperature profile (left) and the 2D temperature profile along a slice in the middle of the domain (right)

5.5 Parameter Estimation

There are some uncertainties in the experimental measurements, such as the inlet temperature and the inlet velocity. The inlet temperature of the premixed stream can be affected by the burner ports which are narrow and tall (1.5 mm $\times$ 2.5 mm wide and 12 mm tall). The port walls are made of stainless-steel and can heat up during the operation of the burner. The velocity is difficult to measure because we can control the overall flow rate of the premixed stream, which comes out of the ports, but can also seep through the ribbon walls that are pressed together, resulting in a slow co-flow. Additionally, we use LES with a mesh small enough to capture the sub-grid scale eddies and thus require no sub-grid scale model. All these factors require some sort of estimation for the experimental parameters. In this study, we use Dakota [30], an open-source package of mathematical and statistical models that allows us to conduct a parameter estimation study on the ribbon burner simulations.

Since we are solving the Navier Stokes equations, the forward model is non-linear and complicated. We can leverage inverse modeling and use gradient-based algorithms in order to estimate experimental parameters. In order to do that, we used the open-source optimization package from Sandia National Lab, Dakota [30]. In order to do parameter estimation with Dakota, we choose an algorithm and give it a cost function to minimize using a set of parameters and ranges.

We selected a non-linear least squares algorithm that adaptively estimates the Hessian through small perturbations to the parameters [31]. The calibration parameters are given to Dakota with a range for their values and a vector is then given from the experimental dataset. The difference between the experimental dataset and the computational mean centerline temperature values at the corresponding experimental heights is defined as the cost function to be minimized. Using this approach, we are trying to optimize the agreement between the experimental and the simulation results by giving Dakota a starting point for the initial parameters (initial velocity of

1 m/s and initial temperature for the premixed methane-air stream of 600 K) and ranges of values for the parameters. After the initial simulation, Dakota runs a couple of simulations with small perturbations to the initial parameter values and estimates the direction of steepest descent. Using a range of inlet temperatures of 300 K $-$ 800 K and a range of inlet velocities of 0.5 m/s $-$ 1.5 m/s, the solver converged in 33 iterations. The results from the 3D calibration study are shown in Figure 5.5. While we predict the near field region well, the temperature peaks and starts to decrease as we get higher into the domain. This can be attributed to not modeling the full length of the ribbon burner and to using a single-step chemistry model where the heat release is not spread out since the reactions occur rapidly near the inlet. Using this approach, we can approximate the initial parameters for a higher fidelity simulation.

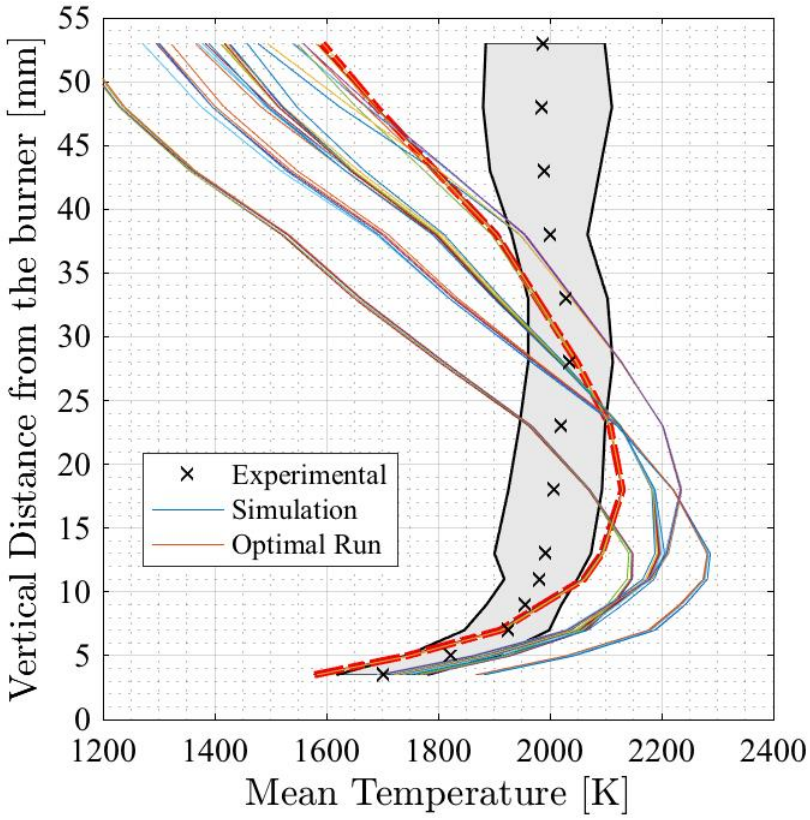

Figure 5.5: Parameter Estimation Using 3D Simulations

5.6 Testing a Higher Fidelity Chemistry Model

In the results shown in the section above, particulary in Figure 5.5, we can see that while the near field prediction of the temperature can be captured using the calibration approach, we do not match the slope of the temperature profile higher up in the domain. One of the main reasons we see this mismatch is due to the chemistry modeling. Using a higher fidelity model, such as the 16 species, 40 step model developed by Yang and Pope [2], we can run a test case to see how accurately we can predict the temperature profile higher up in the domain. Figure 5.6 shows that even for a non-calibrated case, we do a better job in matching the slope higher up in the domain. Further improvements in predicting the experimental temperature profile can be obtained by running a calibration study using detailed chemistry.

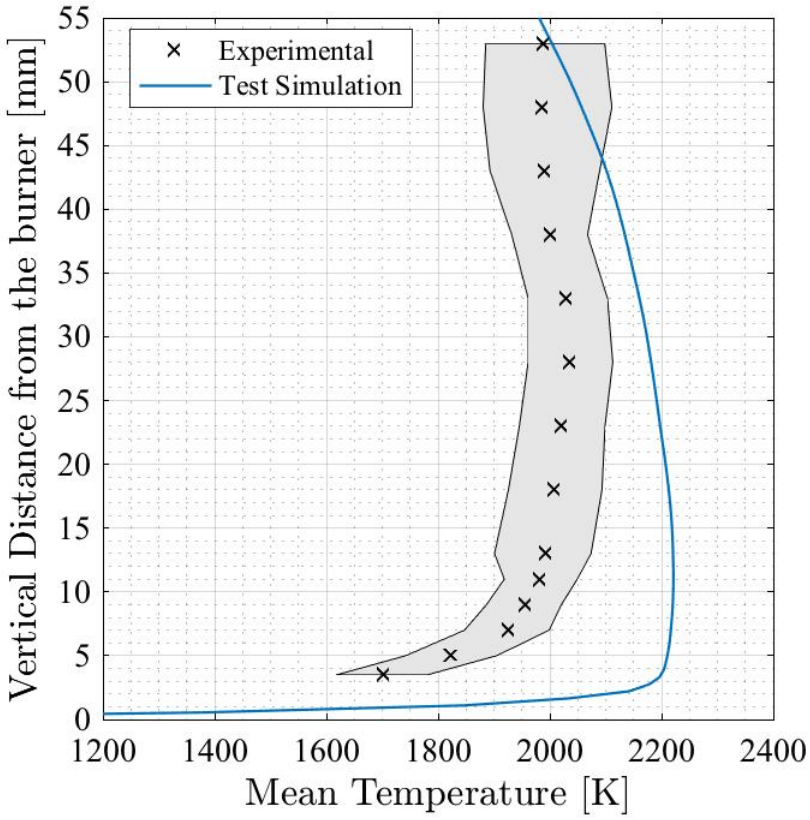

Figure 5.6: Test case with a higher fidelity chemistry model for the ribbon burner

5.7 Analysis of the Puffing Frequency

The flame has a characteristic pulsating behavior shown in the puffing of temperature and velocity fields in the domain. We can quantify the rate of this behavior by looking at the fast fourier transform (FFT) of a point above the burner. Using the base parameter estimation simulation, we can see that there is a distinct peak in the FFT shown in Figure 5.7. This shows that the flow is periodic and can help us characterize the temperature variation. The frequency of this characteristic puffing is 20.1 Hz, which matches closely with a frequency of 19.7 Hz that should be observed for a rectangular inlet with the same dimensions as the ribbon burner. This relation comes from a regression analysis for rectangular inlets based on the experimental results from Cetegen et. al. [32]. This also suggests that the ribbon burner behaves like a rectangular inlet in terms of the pulsating behavior even though the ports give it an intricate geometry.

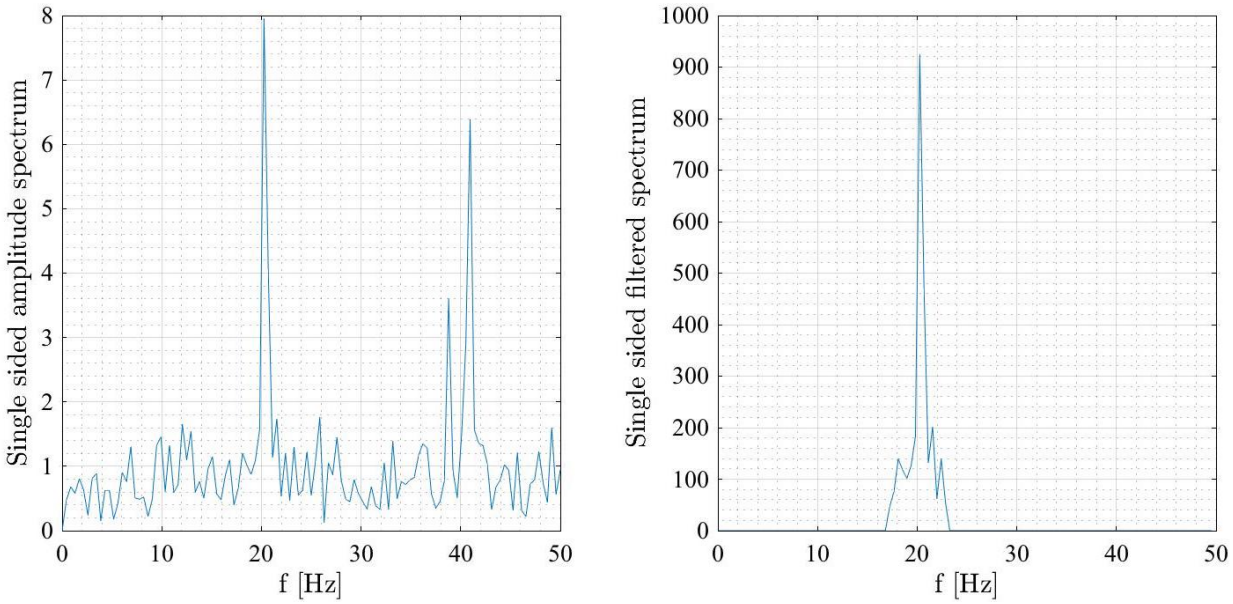

Figure 5.7: Fast fourier transform of the temperature signal (left) and the filtered temperature signal (right) at y = 1.25 cm

For the catalytic burner, this puffing is seen experimentally as well. However, for the ribbon burner, we can see some puffing behavior visually, but it is difficult to obtain numerically since it is hypothesized that the temperature variations are lower than the machine precision of the measurement apparatus. In order to test the hypothesis, we can filter the FFT from Figure 5.7 and analyze the frequency content near the peak of 20 Hz. The right half of Figure 5.7 shows the filtered FFT where we pass all frequency content between 17 Hz and 23 Hz and filter out the rest. We can then invert that FFT and back out the magnitude of the temperature fluctuations from that frequency range. Figure 5.8 shows the plot of temperature at y = 1.25 cm on the centerline over 2.5 s. We can see that all the temperature fluctuations lie within 60 K, which would be the 3% instrumentation accuracy for a temperature range of around 2000 K. Thus, the lack of distinct peaks in the FFT of the experimental data can be attributed to the accuracy of the measurements.

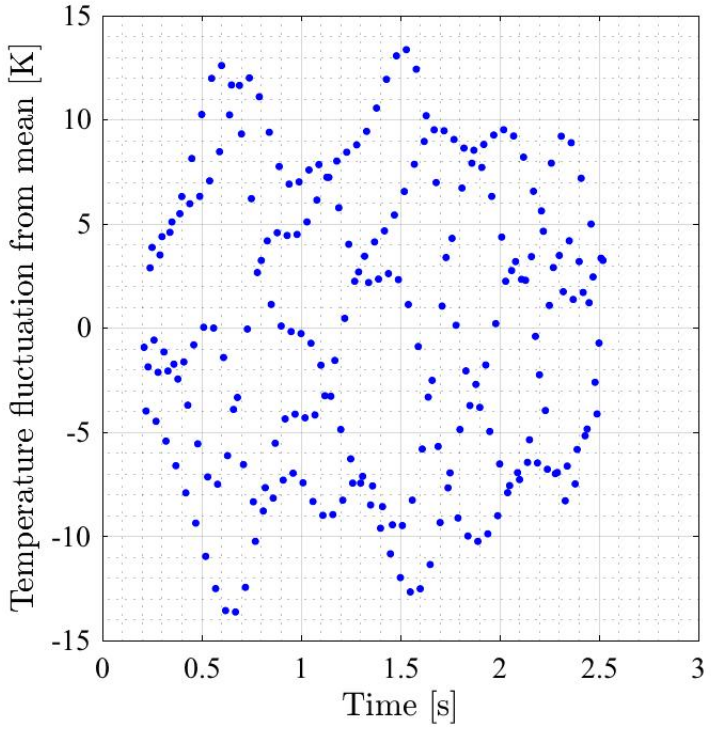

Figure 5.8: Temperature fluctuations around the mean from the filtered values at y = 1.25 cm

Chapter 6

Summary

6.1 Project Summary

This project builds on the respective computational and experimental strengths of the PIs, in addition to leveraging prior long-term research support from 3M. In the past two years, the experimental test stand has been designed and manufactured, the absorption laser diagnostics have been developed and validated, and the computational tool has been developed and used in preliminary studies to explore the effect of different system parameters on the temperature field at the film surface. In all research, a specific emphasis has been placed on determining temperature uniformity and radical concentrations above the burner.

In this thesis, we studied the effect of additional unreacted fuel in the domain above the catalytic burner. We also looked at the initial results from the parameter estimation study for the ribbon burner, which show that this method can be useful to calibrate for parameters that might be hard to obtain experimentally. Using a gradient-based approach reduces the number of total simulations that need to be performed and provides an understanding of the sensitivity of each parameter to the centerline temperature profile. Preliminary studies of this parameter space have been performed for relatively simple reaction models, but now the complexity of the reaction models must be increased in order to improve physical realism and to compare with the experimental results obtained by the researchers participating in this joint effort for 3M.

6.2 Areas for Improvement

Potential drawbacks of the FireFOAM solver are the ability to predict fluid velocities, flame height, and entrainment of air. Wang et. al. [7] show that their solver under-predicts the velocities compared to the experiments. The flame height is difficult to measure experimentally because of the dependence on intermittency and the luminous flame burnout. The authors define flame height as the temporal average of the highest location in the domain where the stoichiometric mixture exists. This definition is different from the experimental measure and the uncertainty of experimental data makes it even more difficult to extract.

Another avenue for improvement of FireFOAM and OpenFOAM is in the chemistry modeling. When simulating chemical reactions (such as the combustion of a premixed methane jet), often an advanced chemistry mechanism is used that tracks several species. Currently, the transport properties for all the species are assumed to be equal and it is non-trivial to change those values. Capturing those transport properties accurately is important for the species and temperature propagation in the domain. While look-up tables (another popular method of simulating chemical interactions in reacting flow simulations) are implemented in OpenFOAM v5, it is still not trivial to change the transport properties. Using an augmented reduced mechanism [33] and better modeling of the species transport properties, we can improve the accuracy of the simulation while still introducing a lot fewer species than the GRI 3.0 mechanism. This will strike a balance between the computational cost and the accuracy of the simulations.

6.3 Future Work

We have started to use a new mesh modification method to further reduce the cost of our simulations. Adaptive mesh refinement (AMR) is a technique used in several finite volume solvers and it has been developed for FireFOAM by a student in the Turbulence and Energy Systems Laboratory, Caelan Lapointe.

Physically, AMR modifies the mesh regularly at a frequency defined by the user and based on fields also defined in the solver by the user. This allows us to refine our mesh by splitting one cell into eight cells. For example, in our initial AMR ribbon burner simulation, the solver checks the domain for cells that have a temperature higher than 600 K after every ten time-steps, and refines those cells while bringing the cells that have temperatures below 600 K back to the original coarse size. Using this technique allows us to start with a coarse mesh and refine along any field as required, therefore allowing us to get the same effective resolution as a static mesh but with fewer cells. For the initial simulation, we modeled 60% of the ribbon burner length assuming a rectangular inlet. Figure 6.1 shows the progression of an AMR solver through time.

During the next two years, the experimental measurement library will be expanded, the physical fidelity of the computational tool will be increased, and the experimental and computational data will be used in a coupled, integrated approach to understanding catalytic burner operation and build upon the understanding of the ribbon burner operation. In future years, this research platform may be used to examine optimization and control of the combined burner/chilled-roll system, as well as make detailed comparisons between catalytic and ribbon burners.

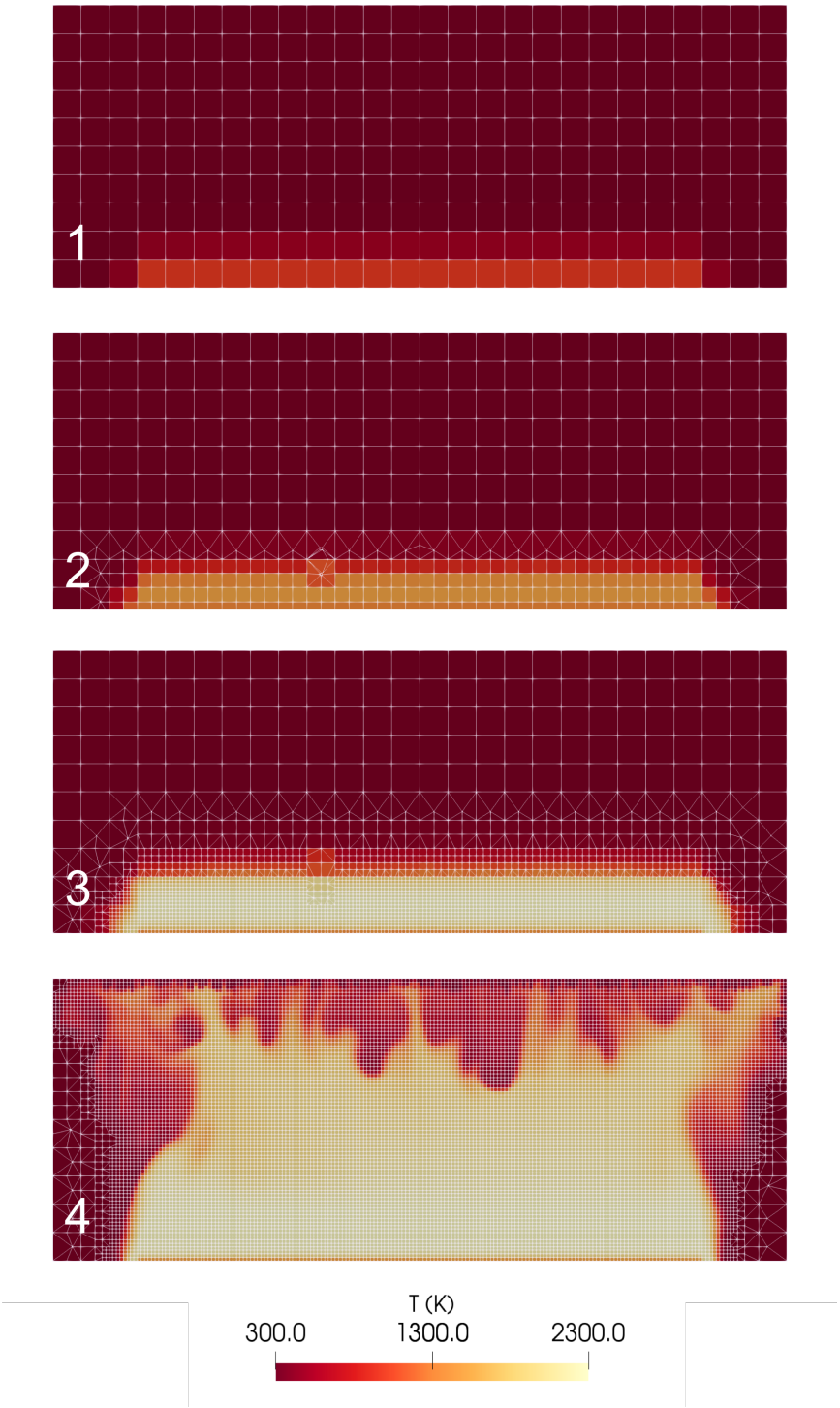

Figure 6.1: Demonstration of AMR for the ribbon burner by visualizing the mesh in a slice at the center of the domain running across the length of the burner. (1) No AMR, base resolution is coarse at t = 0.01 s. (2) First level of AMR at t = 0.02 s. (3) Maximum refinement with AMR at t = 0.03 s. (4) Mesh after the flow has developed at t = 1 s.

6.4 Impact

The overall impact of this research is on the optimization and improvement of burner/chilled-roll systems for polymer film flame treatments. Using the experimental and computational tools developed in this project, existing treatment processes will be improved and new avenues of technology innovation will be explored.

Through the work shown in this thesis, my contributions to the computational effort are that:

- I showed that even small amounts of unreacted fuel (CH_4) entering the domain above the catalytic burner can have a significant impact on the temperature profiles and could potentially explain the higher temperature magnitudes seen in the experimental data.
- I tested several different meshing techniques, chemistry models, and turbulence solvers.
- I conducted a parameter estimation study on the ribbon burner, wherein an open-source parameter optimization and calibration toolkit, Dakota, was used. A non-linear least squares algorithm was used to infer inlet parameters (temperature and velocity) for optimized matching with the experimental temperature profile.
- I tested new development softwares from our laboratory such as the adaptive mesh refinement enabled FireFOAM solver.

Bibliography

[1] Hrvoje Jasak, Aleksandar Jemcov, Zeljko Tukovic, et al. Openfoam: A c++ library for complex physics simulations. In International workshop on coupled methods in numerical dynamics, volume 1000, pages 1–20. IUC Dubrovnik, Croatia, 2007.

[2] B Yang and SB Pope. Treating chemistry in combustion with detailed mechanismsfi?!in situ adaptive tabulation in principal directionsfi?!premixed combustion. Combustion and Flame, 112(1-2):85–112, 1998.

[3] Colleen Stroud, Melvyn C Branch, Trina Vian, Neal Sullivan, Mark Strobel, and Michael Ulsh. Characterization of the thermal and fluid flow behavior of industrial ribbon burners. Fuel, 87(10-11):2201–2210, 2008.

[4] Norbert Peters. Turbulent combustion. Cambridge university press, 2000.

[5] Thierry Poinsot and Denis Veynante. Theoretical and numerical combustion. RT Edwards, Inc., 2005.

[6] Isabella Mazza, Ahmet Duran, Yakup Hundur, Cristiano Persi, Andrea Santoro, and Mehmet Tuncel. Scalability of openfoam for simulations of a novel electromagnetic stirrer for steel casting. In Proceedings of the International Conference on Parallel and Distributed Processing Techniques and Applications (PDPTA), page 111. The Steering Committee of The World Congress in Computer Science, Computer Engineering and Applied Computing (WorldComp), 2016.

[7] Yi Wang, Prateep Chatterjee, and John L de Ris. Large eddy simulation of fire plumes. Proceedings of the Combustion Institute, 33(2):2473–2480, 2011.

[8] Werner J. A. Dahm and Peter E. Hamlington. Introduction to Turbulence and Turbulent Flows: Physical Concepts, Statistical Theory, and Modeling. 2017.

[9] Ashwani K Gupta, David G Lilley, and Nick Syred. Swirl flows. Tunbridge Wells, Kent, England, Abacus Press, 1984, 488 p., 1984.

[10] John Harrison Konrad. An experimental investigation of mixing in two-dimensional turbulent shear flows with applications to diffusion-limited chemical reactions. PhD thesis, California Institute of Technology, 1977.

[11] WPa Jones and JH Whitelaw. Calculation methods for reacting turbulent flows: a review. Combustion and flame, 48:1–26, 1982.

[12] Francisco E Hernández Pérez, Nurzhan Mukhadiyev, Xiao Xu, Aliou Sow, Bok Jik Lee, Ramanan Sankaran, and Hong G Im. Direct numerical simulations of reacting flows with detailed chemistry using many-core/gpu acceleration. Computers & Fluids, 2018.

[13] Feichi Zhang, Henning Bonart, Thorsten Zirwes, Peter Habisreuther, Henning Bockhorn, and Nikolaos Zarzalis. Direct numerical simulation of chemically reacting flows with the public domain code openfoam. In High Performance Computing in Science and Engineering fi14, pages 221–236. Springer, 2015.

[14] Jürgen Warnatz, Ulrich Maas, and Robert W Dibble. Physical and Chemical Fundamentals, Modeling and Simulation, Experiments, Pollutant Formation. Springer, 1995.

[15] Stephen B Pope. Turbulent flows, 2001.

[16] Henning Bonart. Implementation and validation of a solver for direct numerical simulations of turbulent reacting flows in OpenFOAM. PhD thesis, Bachelorfis thesis, Karlsruhe Institute of Technology, 2012.

[17] Keith J Laidler. The development of the arrhenius equation. Journal of Chemical Education, 61(6):494, 1984.

[18] Gregory P Smith, David M Golden, Michael Frenklach, Nigel W Moriarty, Boris Eiteneer, Mikhail Goldenberg, C Thomas Bowman, Ronald K Hanson, Soonho Song, William C Gardiner Jr, et al. Gri 3.0 mechanism. Gas Research Institute, Des Plaines, IL, accessed Aug, 21:2017, 1999.

[19] FM Global. Firefoam. FM Global, 2014.

[20] Kevin McGrattan, Simo Hostikka, Jason Floyd, Howard Baum, Ronald Rehm, William Mell, and Randall McDermott. Fire dynamics simulator (version 5), technical reference guide. NIST special publication, 1018(5), 2004.

[21] JP OfiSullivan, RA Archer, and RGJ Flay. Consistent boundary conditions for flows within the atmospheric boundary layer. Journal of Wind Engineering and Industrial Aerodynamics, 99(1):65–77, 2011.

[22] Jonathon Anderson, Patrick J Burns, Daniel Milroy, Peter Ruprecht, Thomas Hauser, and Howard Jay Siegel. Deploying rmacc summit: an hpc resource for the rocky mountain region. In Proceedings of the Practice and Experience in Advanced Research Computing 2017 on Sustainability, Success and Impact, page 8. ACM, 2017.

[23] Thierry Poinsot and Denis Veynante. Theoretical and numerical combustion. RT Edwards, Inc., 2005.

[24] BJ McCaffrey. Purely buoyant diffusion flames: Some experimental results. final report. Chemical and Physical Processes in Combustion. The National Institute of Standards and Technology (NIST), Miami Beach, page 49, 1979.

[25] H Jasak. Error analysis and estimation for the finite volume method with applications to fluid flows. thesis submitted for the degree of doctor. department of mechanical engineering, imperial college of science, 1996. 1996.

[26] Howard R Baum, Kevin B McGrattan, and Ronald G Rehm. Three dimensional simulations of fire plume dynamics. Fire Safety Science, 5:511–522, 1997.

[27] TG Ma and JG Quintiere. Numerical simulation of axi-symmetric fire plumes: accuracy and limitations. Fire Safety Journal, 38(5):467–492, 2003.

[28] Gunnar Heskestad. Fire plumes, flame height, and air entrainment. In SFPE handbook of fire protection engineering, pages 396–428. Springer, 2016.

[29] CEA NASA. Chemical equilibrium with applications. Software Package, Ver, 2.

[30] Brian M Adams, WJ Bohnhoff, KR Dalbey, JP Eddy, MS Eldred, DM Gay, K Haskell, Patricia D Hough, and Laura P Swiler. Dakota, a multilevel parallel object-oriented framework for design optimization, parameter estimation, uncertainty quantification, and sensitivity analysis: version 5.0 userfis manual. Sandia National Laboratories, Tech. Rep. SAND2010-2183, 2009.

[31] JE Dennis, DM Gay, and RE Welsch. Algorithm 573: Nl2sol. An adaptive non, 1981.

[32] BM Cetegen, Y Dong, and MC Soteriou. Experiments on stability and oscillatory behavior of planar buoyant plumes. Physics of Fluids, 10(7):1658–1665, 1998.

[33] CJ Sung, CK Law, and J-Y Chen. An augmented reduced mechanism for methane oxidation with comprehensive global parametric validation. In Symposium (International) on Combustion, volume 27, pages 295–304. Elsevier, 1998.